

1  
2  
3  
4  
5  
6  
7  
8  
9  
10  
11  
12  
13  
14  
15  
16  
17

**A consistent ocean oxygen profile dataset with new quality control and bias assessment**

Viktor Gourteski<sup>1,\*</sup>, Lijing Cheng<sup>1,\*</sup>, Juan Du<sup>1</sup>, Xiaogang Xing<sup>2</sup>, Fei Chai<sup>3,4</sup>, Zhetao Tan<sup>1</sup>

<sup>1</sup> Institute of Atmospheric Physics, Chinese Academy of Sciences, Beijing, China

<sup>2</sup> State Key Laboratory of Satellite Ocean Environment Dynamics, Second Institute of Oceanography, Ministry of Natural Resources, Hangzhou, China

<sup>3</sup> State Key Laboratory of Marine Environmental Science, Xiamen University, Xiamen, China

<sup>4</sup> College of Ocean and Earth Sciences, Xiamen University, Xiamen, China

*Correspondence to:* Viktor Gouretski ([viktor.gouretski@posteo.de](mailto:viktor.gouretski@posteo.de)); Lijing Cheng ([chenglij@mail.iap.ac.cn](mailto:chenglij@mail.iap.ac.cn))

18 **Abstract.** The global ocean oxygen concentrations have declined in the past decades, posing threats  
19 to marine life and human society. High-quality and bias-free observations are crucial to  
20 understanding the ocean oxygen changes and assessing their impact. Here, we propose a new  
21 automated quality control (QC) procedure for ocean profile oxygen data. This procedure consists of  
22 a suite of ten quality checks, with outlier rejection thresholds being defined based on underlying  
23 statistics of the data. The procedure is applied to three main instrumentation types: bottle casts,  
24 CTD (Conductivity-Temperature-Depth) casts, and Argo profiling floats. Application of the quality  
25 control procedure to several manually quality-controlled datasets of good quality suggests the  
26 ability of the scheme to successfully identify outliers in the data. Collocated quality-controlled  
27 oxygen profiles obtained by means of the Winkler titration method are used as unbiased references  
28 to estimate possible residual biases in the oxygen sensor data. The residual bias is found to be  
29 negligible for electrochemical sensors typically used on CTD casts. We explain this as the  
30 consequence of adjusting to the concurrent sample Winkler data. Our analysis finds a prevailing  
31 negative residual bias for the delayed-mode quality-controlled and adjusted profiles from Argo  
32 floats varying from  $-4$  to  $-1 \mu\text{mol kg}^{-1}$  among the data subsets adjusted by different Argo data  
33 assembly centers (DACs). The respective overall DAC-specific corrections are suggested. Applying  
34 the new QC procedure and bias adjustment resulted in a new global ocean oxygen dataset from  
35 1920 to 2023 with consistent data quality across bottle samples, CTD casts, and Argo floats. The  
36 adjusted Argo profile data is available at the Marine Science Data Center of the Chinese Academy  
37 of Sciences (Gouretski et al., 2023, <http://dx.doi.org/10.12157/IOCAS.20231208.001>)

## 39 **1 Introduction**

40 Progressive warming caused by the human-induced increase of the greenhouse gases in the  
41 Earth's atmosphere leads to the decline of the dissolved oxygen concentration in the global ocean  
42 because of the reduction in oxygen solubility, the increase in stratification, which hampers the  
43 exchange between the surface layer and the ocean interior, and the accompanying change of ocean  
44 circulation (Keeling et al., 2010; Gruber et al., 2011; Deutsch et al., 2011; Praetorius et al., 2015;  
45 Oschlies et al., 2018). Another factor related to human activities is the increasing input of nutrients  
46 from agriculture and wastewater in the coastal regions (Oschlies et al., 2018; Breitburg et al., 2018).  
47 Nutrients facilitate the growth of phytoplankton and microbes subsequently decrease oxygen levels  
48 after the phytoplankton dies (Breitburg et al., 2018; Pitcher et al., 2021).

49 Recognizing the crucial role of dissolved oxygen for marine aerobic organisms, oceanographers  
50 started to measure oxygen in the late 19<sup>th</sup> century using the chemical method developed by Winkler

51 (1888). Since then, Winkler titration has been a standard method used on oceanographic ships and  
52 in laboratories (Langdon, 2010), and the technique has an accuracy estimated to be 0.1% or  $\pm 0.3$   
53  $\mu\text{mol kg}^{-1}$  (Carpenter, 1965).

54 With the rapid technological progress during the 1960-70s and the development of the  
55 electronic CTD (Conductivity-Temperature-Depth) profilers, the first electrochemical sensors  
56 appeared, providing the possibility for continuous oxygen profiling, which is not possible with the  
57 Winkler method restricted by water samples from several depth levels. Electrochemical sensors are  
58 based on a Clark polarographic membrane (Clark et al., 1953). Oxygen concentration outside the  
59 membrane and oxygen diffusion through the membrane determine the sensor response.  
60 Electrochemical Clark-type sensors possess a very fast time response ( $<1$  s), with an initial accuracy  
61 of 2% of oxygen saturation and precision of about  $1 \mu\text{mol kg}^{-1}$  (Coppola et al., 2013). However,  
62 sensor drift due to fouling and electrolyte consumption over time requires periodic calibration. The  
63 first type of sensors applied on Biogeochemical Argo profiling floats (BGC floats) were Clark-type  
64 electrodes (Riser and Johnson, 2008).

65 Optical oxygen sensors called “optodes” are based on the principle of fluorescence quenching  
66 of a fluorescent indicator embedded in a sensing foil (Körtzinger et al., 2005, Tengberg et al., 2006).  
67 The optode sensors appeared soon after the first implementation of the Clark-type sensors on Argo  
68 floats (Gruber et al., 2010). Compared to electrochemical sensors, optodes are characterized by  
69 long-term stability and high precision with the disadvantage of a slower response time (Gregoire et  
70 al., 2021). During the initial period of several years, both Clarke-type and optode sensors were used  
71 on Argo floats (Claustre et al., 2020). However, drift and initial calibration issues with  
72 electrochemical sensors have led to the increased implementation of optodes on Argo floats  
73 (Claustre et al., 2020), for which calibration using simultaneous water samples is not possible. From  
74 the beginning of the BGC-Argo float implementation until March 2024, there have been more than  
75 2100 Profiling biogeochemical (BGC) Argo floats that provide ocean oxygen observations with  
76 unprecedented temporal and spatial resolutions in this century (Johnson et al. 2017; Roemmich et  
77 al. 2019).

78 Different techniques have been applied in the past to collect ocean oxygen data, and the total  
79 number of oxygen profile data from all instrument types within the World Ocean Database (Boyer  
80 et al., 2018) reached a total of more than 1.2 million by 2023. However, there are a lot of data  
81 quality issues in the historical oxygen database due to many reasons, including instrumental errors,  
82 data collection failure, data processing errors, improper sample storage, unit conversion and others.  
83 Furthermore, as different instruments have different data quality, merging several instrumentation  
84 types into an integrated database requires proof of data consistency.

85 These quality issues impede the various applications of oxygen data, for instance, investigating  
86 how much oxygen the ocean has lost in the past decades (Levin et al., 2018; Gregoire et al., 2021).  
87 Previous assessments indicate the decline of open ocean full-depth O<sub>2</sub> content of 0.3%~2% since  
88 the 1960s, with an upper 1000 m O<sub>2</sub> content decrease of 0.5–3.3% ( $0.2\text{--}1.2 \mu\text{mol kg}^{-1} \text{dec}^{-1}$ ) during  
89 1970–2010 (Gulev et al. 2023). The maximum estimate is at least 6 times larger than the minimum  
90 one, suggesting substantial uncertainty in quantifying the open ocean oxygen changes, which is a  
91 grand challenge for the accurate assessment of deoxygenation (Helm et al. 2011; Long et al. 2016;  
92 Ito et al. 2017; Schmidtko et al. 2017; Breitburg et al. 2018; Sharp et al. 2023). Furthermore, there  
93 is a mismatch between observed and modelled trends in dissolved upper-ocean oxygen over the last  
94 50 years (Stramma et al. 2012). Uncertainties and differences between estimates are at least partly  
95 attributed to the oxygen data quality issues and inconsistency introduced by different instrument  
96 types (e.g. different precision, instrument-specific errors/biases) (Gregoire et al., 2021). For  
97 example, some BGC-Argo data conduct in-air oxygen measurements, which can be used to correct  
98 potential systematic errors, while in other cases, a climatology is used (i.e. World Ocean Atlas) as a  
99 reference (Bittig and Körtzinger, 2015; Gregoire et al., 2021). Therefore, a consistent and thorough  
100 assessment of oxygen data quality, including uniform data quality control for all instruments and  
101 instrumental bias assessments/corrections, is critical to providing a homogeneous ocean oxygen  
102 database for various follow-on applications, including quantification of the trend of ocean  
103 deoxygenation.

104 The paper aims to provide a quality-controlled (QC-ed), consistent global oxygen dataset for  
105 the entire period 1920-2023. To achieve this goal, a novel automated QC procedure for ocean  
106 oxygen profiles was developed. We implement this QC procedure in the global archive and analyze  
107 and describe the quality of oxygen data obtained by different instrumentation types. The  
108 performance of the quality control procedure is assessed using subsets of high-quality hydrographic  
109 data and the QC-ed BGC Argo float profiles. Finally, we use bottle sample data obtained through  
110 the Winkler method as a reference to assess oxygen biases for ship-based CTD and BGC Argo  
111 oxygen profiles.

112 The rest of the paper is organized as follows. The data and methods employed in the study are  
113 presented in Section 2. The data QC procedure is introduced in Section 3, with the data quality  
114 assessment presented in Section 4. The results of benchmarking the automated QC procedure using  
115 manually controlled datasets are shown in Section 5. Assessment of the residual bias for Argo and  
116 CTD profiles is conducted in Section 6. The impacts of QC and bias adjustment on estimating  
117 oxygen climatology and its changes (including annual cycle and long-term changes) are

118 investigated in Section 7. The results of the study are summarized and discussed in Section 8. Data  
119 and code availability are described in Sections 9 and 10, respectively.  
120

## 121 2 Global archive of dissolved oxygen profiles

122 The original oxygen profile data at observed levels are sourced from two large depositories: 1)  
123 World Ocean Database (WOD) (as of January 2023) and 2) oxygen profiles from the Argo Global  
124 Data Assembly Center (GDAC) (ARGO, 2000). World Ocean Database (Boyer et al., 2018)  
125 represents the largest depository of the dissolved oxygen profile data. For the current study, we used  
126 ship-based WOD oxygen data coming from two main instrumentation types: 1) Ocean Station Data  
127 (OSD) and 2) high-resolution CTD profiles. OSD instrumentation group is represented by bottle  
128 casts with oxygen determined by the Winkler method. CTD profiles are obtained mainly through  
129 the electrochemical sensors. For the Argo float data from GDACs, both raw (unadjusted) and  
130 adjusted and QC-ed data are available with the latter used for the study.

131 The OSD profiles are most abundant between the 1960s to 2000s, CTD profiles between the  
132 1990s to 2010s, and Argo profiles dominate after 2010 (**Fig. 1**). The geographical distribution of  
133 oxygen profiles is inhomogeneous (**Fig. 2**), with OSD profiles exhibiting almost global coverage  
134 compared to CTD and Argo, with dense sampling typical for the near-coastal areas and a sparser  
135 sampling in the central parts of the oceans (**Fig. 2a**). The CTD profiles are most abundant in the  
136 North Atlantic Ocean and are represented by a sparse net of transoceanic sections in the central  
137 parts of the main ocean basins, leaving large data gaps, especially in the central regions of Pacific,  
138 Indian, and Southern oceans (**Fig. 2b**). The total number of profiles from all three groups exceeds  
139 1.2 million for the time period 1920 to 2023, so manual QC of the global oxygen dataset is nearly  
140 impossible.

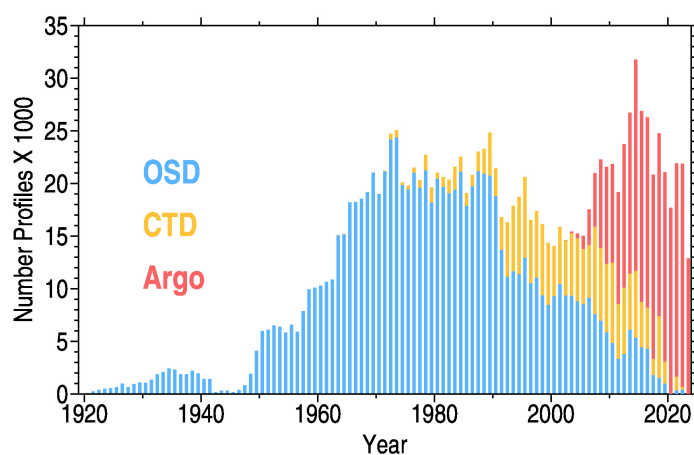


**Figure 1. Yearly number of oxygen profiles from the World Ocean Database (OSD and CTD profiles) and national DACs (Argo) from 1920 to 2023.**

141

142 Amounts of oxygen profiles disseminated by ten national Argo DACs and used for the current  
143 study are given in Table 1. The most considerable contribution comes from two DACs: the Atlantic  
144 Oceanographic and Meteorological Laboratory (AOML) and the French CORIOLIS Center  
145 (Coriolis). Together, these two DACs contribute 71% of all oxygen profiles. The global sampling by  
146 Argo floats is characterized by big gaps in the tropical belt of the World Ocean (**Fig. 2c**) and in the  
147 marginal seas with shallow bottom depths.

148 The DACs report oxygen data along with quality flags set after the QC procedure performed by  
149 each DAC. The spatial distribution of the profiles from each DAC is shown in **Fig. 3**. Only the  
150 AOML dataset is characterized by a more or less global coverage. The profiles from the second  
151 large Coriolis dataset are concentrated mostly in the Atlantic and Southern oceans. Other DACs are  
152 characterized by a regional scope: Japan Meteorological Agency (JMA) data come from the Pacific  
153 Ocean east of Japan, profiles from the Commonwealth Scientific and Industrial Research  
154 Organization (CSIRO) cover the Southern Ocean, China Second Institute of Oceanography (CSIO)  
155 mainly provides Argo profiles from the subtropical and tropical western Pacific Ocean, Argo  
156 profiles from the British Oceanographic Data Centre (BODC) are located in the Atlantic Ocean.  
157 Profiles from the Korea Ocean Research and Development Institute (KORDI) and from Korea  
158 Meteorological Administration (KMA), the smallest two datasets, are located in the southern part of  
159 the Sea of Japan.

160

### 161 **3 Data quality control**

162 Quality evaluation of hydrographic data typically consists of two parts: data QC for random  
163 errors and evaluation of systematic errors or biases. These two issues are often treated separately  
164 but represent the entire QC procedure. A unified QC procedure has yet to be suggested for the  
165 global archive of oxygen profile data, and oxygen-related studies often rely on WOD (Garcia et al.,  
166 2018), Argo (Thierry et al., 2021) and Bushnell et al. (2015) QC procedures. The efforts undertaken  
167 under the International Quality-Controlled Ocean Database (IQuOD) initiative (Cowley, 2021)  
168 resulted in a comprehensive study where different quality control procedures for temperature  
169 profiles were compared and evaluated (Good et al., 2022). As shown in the previous section, the

170 characteristic feature of the global oxygen data archive is its heterogeneity. In the early years, a  
171 relatively small amount of data permitted expert quality control, but for the actual global archive,  
172 automated quality control procedures (AutoQC) are required.

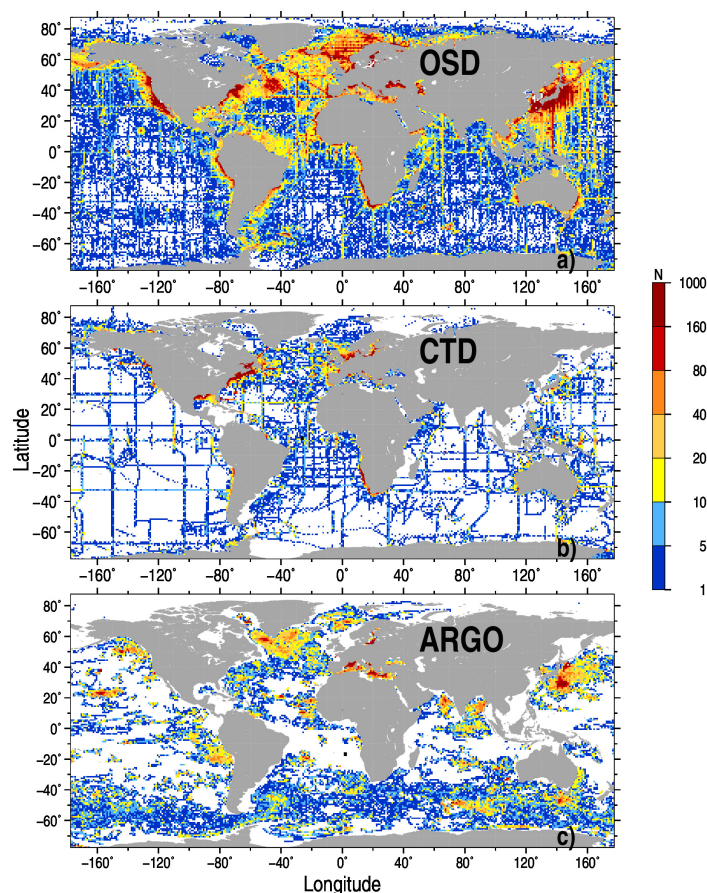


**Figure 2. Number of profiles (N) in 1°×1° latitude/longitude squares for OSD (a), CTD (b), and Argo (c) data.**

173

174 The AutoQC procedure aims to identify and flag outliers, which represent observations  
175 significantly deviating from the majority of other data in the population. Monhor and Takemoto  
176 (2005) noted that there is no rigid mathematical definition of an outlier. The outliers do not  
177 necessarily represent erroneous measurements and can occur due to the natural variability of the  
178 measured variable. A QC procedure defines outliers using a set of thresholds, which are based on  
179 physical laws (for instance, the maximum solubility of gases in the water) or have to be defined  
180 based on the statistical properties of the data population.

181 In this paper, we introduce a novel QC procedure capable of conducting quality assessment of  
182 data from different instrumentation types. The procedure is applied to the observed level data and

183 does not require additional quality checks for profiles interpolated at a predefined set of levels. This  
 184 second level of QC is an attribute of the WOD QC system (Garcia et al., 2018). To increase the  
 185 reliability in detecting erroneous data, a set of quality-checks is applied to each profile. The larger  
 186 the number of failed distinct quality checks, the higher the probability that the flagged observation  
 187 represents a data outlier. Based on the available QC schemes for oceanographic data (most of them  
 188 were developed for temperature and/or salinity profiles), quality checks can be subdivided into the  
 189 following groups:

190 Group-1. Check of location, date and bottom depth of the profile.

191 Group-2. Check of profile attributes (maximum sampled depth, number of levels, variables  
 192 measured) specific to each instrumentation type.

193 Group-3. Range check, e.g., comparison of observations at each level against minimum/maximum  
 194 value thresholds, which are set for the entire ocean or oceanic basin (global ranges) or for the  
 195 particular location and depth.

196 Group-4. Check of the profile shape, which is characterized by the vertical gradient of the  
 197 measured variable at observed levels, by the number of local extrema, and by the presence of  
 198 spikes.

199

200 It should be noted that QC procedures often assume Gaussian distribution law, and outliers are  
 201 defined in terms of multiple times the standard deviation from the mean value (Z-score method).  
 202 For instance, the WOD standard deviation check is based on this assumption (Garcia et al., 2018;  
 203 Boyer et al., 2018). However, distributions of oceanographic parameters are typically skewed, and  
 204 the assumption of Gaussian distribution leads to false data rejection. Tukey (1977) introduced a so-  
 205 called box-plot method, which makes no assumption about the distribution law and is often used for  
 206 outlier detection. Hubert and Vandervieren (2008) developed the adjusted Tukey's boxplot method  
 207 for skewed distribution with fences depending on skewness. Following this approach, Gouretski  
 208 (2018) and Tan et al. (2023) applied QC checks, taking into account the skewness of temperature  
 209 distribution. In the current study we use the Hubert and Vandervieren (2008) adjusted boxplot  
 210 method as modified by Adil and Irshad (2015).

211

212 **Table 1.** Argo oxygen profiles from different national DACs.

N	National Data Assembly Center	Code Name	Number of Argo profiles	Number of Argo profiles	Percent of Argo profiles having
---	-------------------------------	-----------	-------------------------	-------------------------	---------------------------------

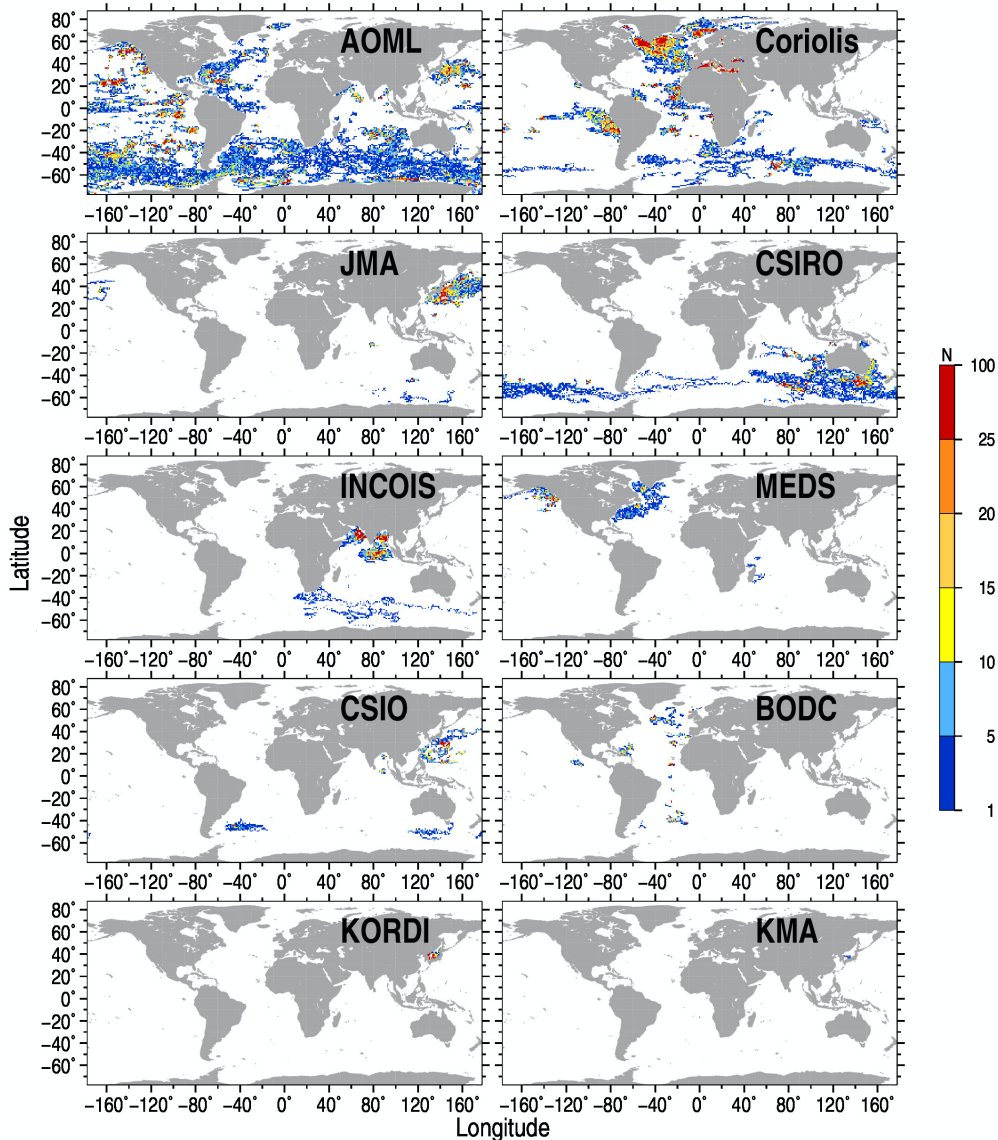


				collocated with Winkler profiles	collocations with Winkler profiles
1	Atlantic Oceanographic and Meteorological Laboratory, US	AOML	89059	32396	41.08
2	CORIOLIS data Center, France	Coriolis	63220	33233	65.09
3	Commonwealth Scientific and Industrial Research Organization, Australia	CSIRO	19183	3302	23.75
4	Japan Meteorological Agency, Japan	JMA	15981	11233	82.90
5	Indian National Centre for Ocean Information Services, India	INCOIS	9901	2069	33.09
6	Second Institute of Oceanography, Ministry of Natural Resources, China	CSIO	6455	3921	68.98
7	Marine Environmental Data Service, Canada	MEDS	4605	14.04	50.50
8	British Oceanographic Data Center, UK	BODC	3533	1905	61.57
9	Korea Ocean Research and Development Institute, Korea	KORDI	2239	0	0
10	Korea Meteorological Administration, Korea	KMA	93	0	0

213

214        Developing the QC procedure, consisting of a suite of distinct checks, we assume that oxygen  
215 data obtained by the reference Winkler method are superior in quality compared to the sensor data.  
216 As noted by Golterman (1983), the principle of the Winkler method has been unchanged since its  
217 introduction, with the method still providing the most precise determination of dissolved oxygen.  
218 There is a total of ten distinct quality checks, which are introduced in sections 3.1 to 3.9. The outlier  
219 statistics are shown in the respective supplements (**Fig. S1-Fig. S10**), both for the year/depth bins  
220 and within 2°×4° geographical boxes and for randomly selected oxygen profiles affected by the  
221 respective check.

222



224 **Figure 3. The number (N) of Argo oxygen profiles in  $1^\circ \times 1^\circ$  spatial boxes for the datasets from**  
 225 **different DACs. The name abbreviation of each DAC is also presented in each panel.**

226

### 227 3.1 Geographical Location Check

228 A comparison of the deepest sampled level with the local ocean bottom depth may be used for  
 229 the identification of erroneous geographical locations. We use GEBCO 0.5-minute resolution digital  
 230 bathymetry map to define thresholds for this check. For each profile, the range between minimum  
 231 and maximum GEBCO bottom depth within the 111 km radius is calculated. If the difference  
 232 between the deepest profile measurement depth and the local GEBCO depth exceeds the above  
 233 depth range, the geographical coordinates of the profile are considered to be in error and data at all

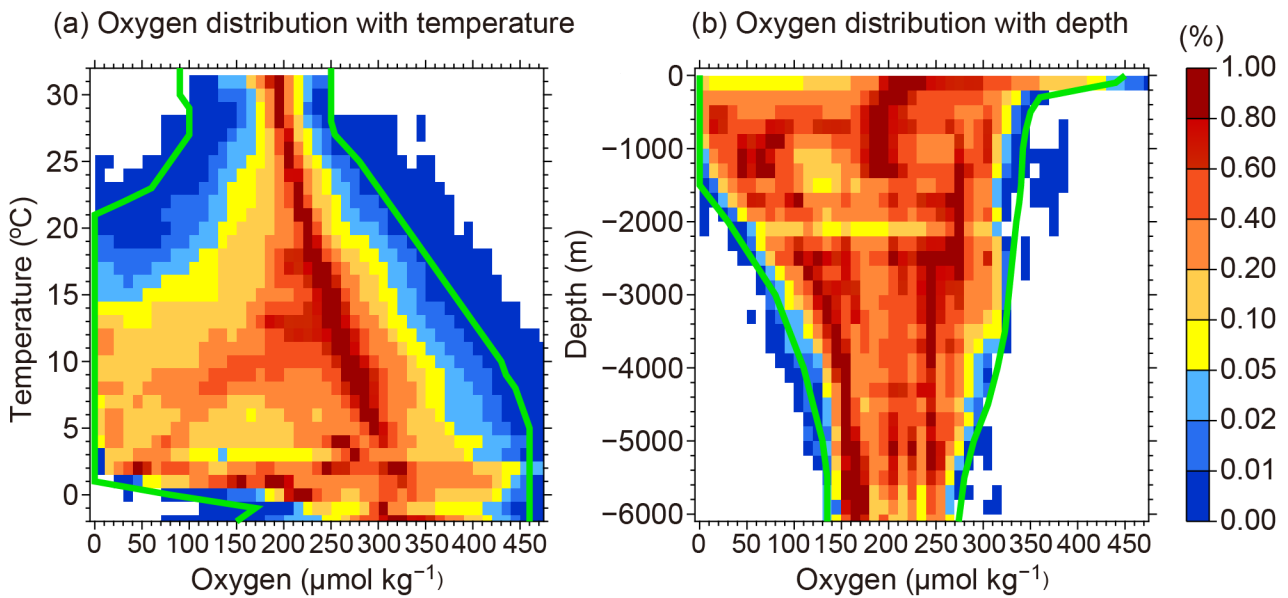
234 levels are flagged. According to Table 2, about 0.5% of OSD and CTD profiles fail this check,  
235 compared to only 0.08% for Argo profiles. For each data type, the spatial distribution of profiles  
236 failing this test exhibits a rather random pattern (**Fig. S1**). The highest percentage of OSD outlier  
237 profiles are found for the time period before 1946, probably due to less accurate navigation methods  
238 during the war (**Fig. S1b**). CTD profiles exhibit higher outlier scores above 400 m between 200-  
239 2014 linked to several cruises. Only 0.077% of DAC QC-ed Argo profiles fail this check (**Fig. S1g-**  
240 **i**).

241

### 242 **3.2 Global oxygen range check**

243 The test is applied to identify observations that are grossly in error (the so-called ‘blunders’).  
244 These data correspond to the cases of the total instrumentation fault or crude errors introduced  
245 during the data recording or formatting. The overall minimum/maximum oxygen ranges are defined  
246 based on the entire archive of the OSD profiles. These overall ranges are set for depth levels and  
247 temperature surfaces because the maximum oxygen solubility depends on temperature. For the  
248 construction of overall limits, we use the normalized frequency histograms (**Fig. 4**). The  
249 depth/oxygen histograms are constructed similarly with normalization at each depth level (**Fig. 4b**).  
250 The normalization is done to account for varying numbers of oxygen observations with depth and  
251 temperature. The relative frequencies serve as the guidance to produce the overall oxygen minimum  
252 and maximum limits, which approximately correspond to the relative frequency of 0.05 (indicated  
253 by the green lines). Spatial distribution of the OSD and CTD profiles with levels failing this check  
254 broadly corresponds to the sampling density (**Fig. S2a, d and Fig. S3a, d**), whereas flagged Argo  
255 profiles can be rather linked to distinct floats (**Fig. S2g, Fig. S3d**). The CTD data are characterized  
256 by the largest fraction of profiles affected by this check (**Fig. S2e, Fig. S3e**).

257



258

**Figure 4. Normalized oxygen histograms used to define overall oxygen ranges versus temperature (a) and versus depth (b). Minimum and maximum overall oxygen limits are shown by solid green lines. For each temperature/oxygen bin in (a), the number of oxygen observations is divided by the number of observations in the most populated bin for the same temperature. The depth/oxygen histograms (b) are constructed similarly with normalization at each depth level.**

259

### 260 3.3 Maximum oxygen solubility check

261 According to Henry's law, the quantity of an ideal gas that dissolves in a definite volume of  
 262 liquid is directly proportional to the partial pressure of the gas. It is also known that gas solubility in  
 263 the water typically decreases with increasing temperature. The histograms of observed oxygen  
 264 concentration ( $C_{\text{obs}}$ ) versus maximum oxygen solubility ( $C_{\text{max}}$ ) calculated using reported  
 265 temperature and salinity at different ocean layers depict a close relationship between the mode of  
 266 observed oxygen distribution and the maximum solubility (**Fig. 5a-d**). The histograms also show  
 267 that the distribution mode for the upper-most layer 0-100 m (**Fig. 5a**) follows the line  $C_{\text{obs}} = C_{\text{max}}$   
 268 progressively deviating to lower  $C_{\text{max}}$  values when  $C_{\text{obs}} > 300 \mu\text{mol kg}^{-1}$ , suggesting an oxygen  
 269 super-saturation. That is because in the photic layer of the ocean oxygen is produced by  
 270 phytoplankton through photosynthesis, and oxygen super-saturation can evolve. Oxygen production  
 271 due to photosynthesis leads to the formation of small bubbles (10-70 micron) with increasing  
 272 oxygen super-saturation accompanied by a higher number of bubbles and their shift towards large  
 273 sizes (Marks, 2008). In the deeper layers (**Fig. 5b-d**), the number of cases with super-saturation

274 decreases because of the reduced photosynthesis, so the temperature and pressure effects dominate.  
 275 According to the histograms (Fig. 5a-d), supersaturation is frequently observed in the upper layers.  
 276 The percentage of supersaturated values decreases from about 45 % in the near-surface layer to less  
 277 than 1.0 % below the 200 m level (Fig. 5e, red).  
 278

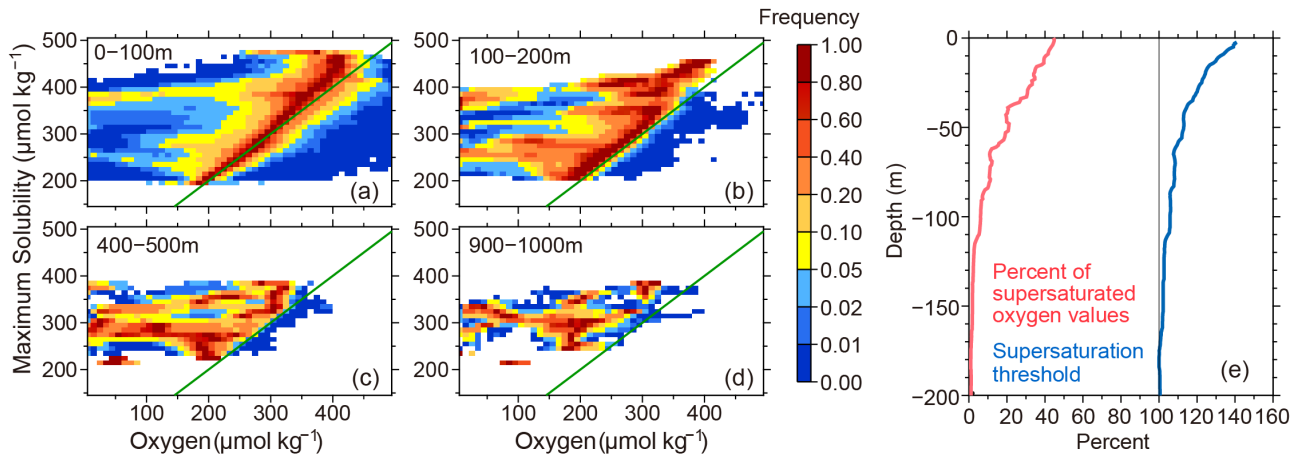


**Figure 5. Super-saturation check: (a-d) normalized frequency histograms for maximum solubility versus reported dissolved oxygen value for different layers. The bin size is  $10 \mu\text{mol kg}^{-1}$ . For each maximum solubility level, the frequencies for each bin are normalized by the number of the values in the most populated bin in order to account for variations in the number of profiles. (e) percentage of supersaturated oxygen values over all observed oxygen values (red) and the threshold for the super-saturation check, represented by the percentage relative to the maximum solubility (blue).**

279  
 280 In order to set the threshold percentage for super-saturation, we calculated histograms of super-  
 281 saturation values for each 1-meter depth level of the upper 500 m layer. The threshold percentage of  
 282 super-saturation (Fig. 5e, blue line) corresponds to the 99th quantile. The threshold value  
 283 approaches 100% near the depth of 200m, therefore, below 200 m all supersaturated oxygen values  
 284 are flagged. Locations of profiles with at least one observed level failing this check are shown in  
 285 Fig. S4a, d, g. The distribution of profiles broadly corresponds to the spatial sampling density. The  
 286 OSD outliers are more numerous in the early years before 1955 probably pointing to less accurate  
 287 measurements during that time period. The check reveals a much higher percentage of CTD outliers  
 288 throughout the water column for several years before 2000 (Fig. S4b) compared to other  
 289 instrumentation types. Argo floats are characterized by the low outlier percentage for this quality

290 check with a higher percentage found for deep Argo floats between 2017-2018 below 2000m (**Fig.**  
291 **S4h**).

292

### 293 **3.4 Stuck value check**

294 Malfunctioning of sensors often results in stuck values when the same oxygen concentration is  
295 reported for all or most of the observed levels. To identify such profiles, we calculated oxygen  
296 standard deviations for each oxygen profile to build histograms (**Fig. 6**) for each instrumentation  
297 type. Only profiles with at least seven oxygen levels are considered. Unlike the OSD and Argo data,  
298 for which the frequency of profiles drops for low standard deviation values, the CTD profiles are  
299 characterized by a distinct peak for the lowest standard deviation values (**Fig. 6c**). Accordingly,  
300 based on the histograms (**Fig. 6b, c**), we set the thresholds of  $3 \mu\text{mol kg}^{-1}$  and  $1 \mu\text{mol kg}^{-1}$  and for  
301 CTD and Argo profiles, respectively. No lowest value thresholds are applied for OSD profiles, as  
302 stuck values are only characteristics of the electronic sensors. The geographical distribution of  
303 profiles failing this check is given in **Fig. S5 a, d**. The check is applied only to the CTD and Argo  
304 sensor data and reveals a high percentage of outliers for CTD profiles, especially after 2000 (**Fig.**  
305 **S5b**). Argo profiles which fail the check are not numerous and are located mostly in the Northern  
306 Hemisphere (**Fig. S5d**).

307

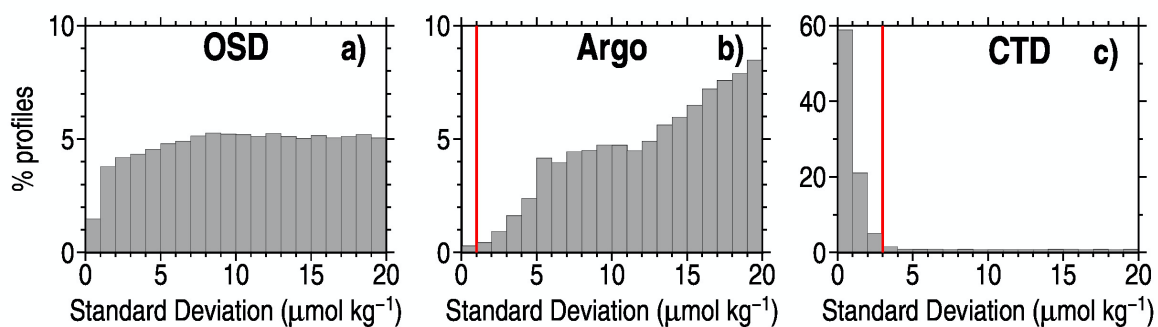


**Figure 6. Oxygen profile standard deviation for OSD (a), Argo (b), and CTD (c) instrumentation types. Only profiles with at least seven levels of oxygen data are considered. Red vertical lines show the respective threshold values for Argo and CTD profiles.**

308

### 309 **3.5 Multiple extrema check**

310 Multiple extrema check aims to identify profiles whose shape significantly deviates from the  
311 majority of profiles. For each profile with at least 7 observed levels (black dots), the number of

312 local extrema and their magnitudes (denoted as  $M_n$  in **Fig. 7a**, defined as oxygen difference  
 313 between two adjacent oxygen measurements) are calculated. Then, the normalized frequency  
 314 histograms of oxygen profiles for different combinations of the number of oxygen extrema and of  
 315 the extremum magnitude are calculated for three instrumentation types separately (**Fig. 7b-d**). The  
 316 larger the extremum magnitude, the less frequent the corresponding profiles. Physically, an oxygen  
 317 profile at a location is not likely to exhibit too large and too frequent oscillations of oxygen  
 318 concentrations. Thus, the profiles with many/big extrema are likely erroneous. The histogram for  
 319 Argo profiles differs from those for OSD and CTD because it is based on profiles already validated  
 320 by the respective DACs. The Multiple extrema check thresholds (black lines in **Fig. 7b-d**) are  
 321 defined using the histograms as the guidance. The lines crudely correspond to the normalized  
 322 frequency of 0.01 for OSD and CTD and 0.05 for Argo profiles. The geographical distribution of  
 323 profiles failing the check is given in **Fig. S6a, d, g**. Argo profiles failing the check can be linked to  
 324 distinct floats (**Fig. S6g**). The OSD profiles exhibit a higher outlier percentage for the years 1990-  
 325 2002. The highest rejection rate for the CTD profiles is typical for the years before 2000 (**Fig. S6b,**  
 326 **e**).

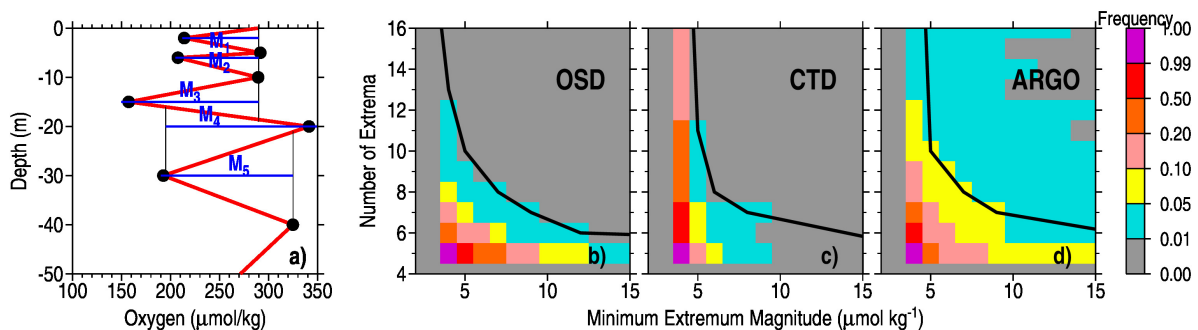


**Figure 7. (a) Schematics for the multiple extrema check. Black dots represent the observed values, and the local extrema is defined by  $M$ , whereas extremum magnitudes are shown with blue lines. (b-d) Normalized frequency histograms for multiple extrema checks for OSD (b), CTD (c), and Argo (d). The area to the right of the black line corresponds to oxygen profiles failing the multiple extrema check.**

327

### 328 3.6 Spike check

329 Spikes are the values at levels that strongly deviate from the values at the nearest levels above  
 330 and below. For each observed level  $k$ , the test value  $s = s_1 - s_2$  is calculated, where  $s_1 = |p_k - 0.5|$  ( $p_{k-1}$ -

331  $p_{k+1})$ ,  $s_2=|0.5 (p_{k+1} - p_{k-1})|$  and  $p$  denotes the oxygen value. The observation is identified as outliers  
 332 when the test value  $s$  exceeds a threshold value. Due to the larger oxygen variability in the upper  
 333 layers, we set depth-dependent spike thresholds, which are defined for nine depth layers using  
 334 accumulated histograms for the test value  $s$  (Fig. 8a, b for 0-100m, 400-600m as examples). The  
 335 threshold profile is defined by the 95% frequency at each layer (Fig. 8c). The value is chosen  
 336 empirically but can be tuned when additional QC-ed benchmark datasets become available.  
 337 Examples of profiles which failed this check are shown in Fig. 7S. Data from all instrument types  
 338 are characterized by a rather homogeneous temporal and spatial distribution of outliers.  
 339

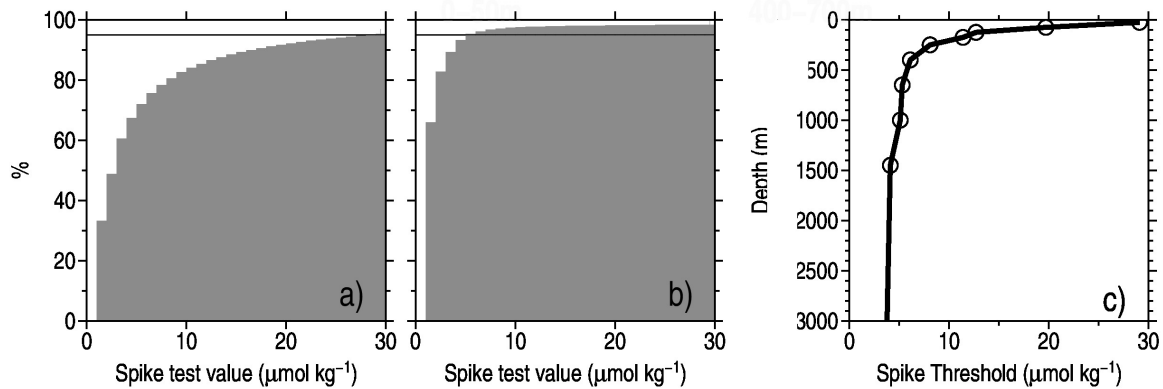


**Figure 8. Spike check value histograms (see text for details) for the layer 0-100m (a) and 400-600m (b); spike check value threshold versus depth (c).**

### 340 3.7 Local climatological oxygen range check

341 Local climatological oxygen range check is one of the most effective QC modules for  
 342 identifying outliers compared to other checks because the minimum/maximum thresholds are  
 343 constrained by the local water mass characteristics. For each  $1^\circ \times 1^\circ$  latitude/longitude grid point, we  
 344 calculate min/max thresholds, accounting for the skewness of the data. For calculating  
 345 climatological ranges, we take the ergodic hypothesis in which the average over time is considered  
 346 to be equal to the average over the data ensemble within a certain spatial influence radius. Taking  
 347 into account the skewness of statistical distribution when defining climatological ranges for  
 348 oceanographic parameters was first suggested by Gouretski (2018), who applied Tukey's box plot  
 349 method modified for the case of skewed distributions (Hubert and Vandervieren, 2008; Adil and  
 350 Irshad, 2015). In this method lower (Lf) and upper (Lu) fences are calculated according to formula  
 351 (1):

352



353  $[L_f \ U_f] = [ Q1 - 1.5*IQR*\exp(-SK*|MC|) \ Q3 + 1.5*IQR*\exp(SK*|MC|) ], \quad (1)$

354

355 where Q1, Q3 are quartiles, Q2 is sample median, SK is skewness. MC denotes medcouple, which  
356 is defined as  $MC = \text{median } h(x_i, x_j)$ , where  $x_i \ll Q2 \ll x_j$ ; and the kernel function  $h(x_i, x_j) = [(x_j - Q2) -$   
357  $(Q2 - x_i)] / (x_j - x_i)$  (Hubert and Vandervieren, 2008).

358 The local oxygen ranges are constructed using both the OSD and Argo oxygen profiles. The  
359 OSD data used to derive the local threshold have undergone the preliminary QC (checks for global  
360 oxygen range, spikes, stuck value, multiple extrema), aiming to remove crude outliers to reduce  
361 their impact on the local thresholds. This approach is similar to the two-stage thresholding  
362 suggested by Yang et al. (2019). The Argo oxygen profiles underwent quality control at the  
363 respective DAC centers.

364 The local minimum and maximum thresholds were calculated at  $1^\circ \times 1^\circ$  grids at a set of 65 depth  
365 levels corresponding to the levels implemented for the World Ocean Circulation Experiment/Argo  
366 Global Hydrographic Climatology (Gouretski, 2018) using formula (1). Examples of the threshold  
367 spatial distribution are presented for two depth levels: 98 meters (level typically located below the  
368 seasonal thermocline, **Fig. 9a-c**) and 1050 m (level typically located below the main thermocline,  
369 **Fig. 9 d-f**). The most striking features are the areas with low minimum oxygen values (oxygen  
370 minimum zones, **Fig. 9 a, b**) in the East Pacific, Arabian Sea, Bay of Bengal, Black Sea, and Baltic  
371 Sea. The oxygen range map for level 98 m (**Fig. 9c**) shows that the areas with the widest local  
372 ranges coincide with minimum oxygen zones. The local range map for the 98 m level also depicts  
373 wider ranges in several highly dynamic regions of the Gulf Stream, Malvinas current, and the area  
374 north of the Antarctic coast (**Fig. 9c**). During the QC, gridded minimum and maximum local oxygen  
375 values are interpolated to the observed levels at profile locations. The geographical distribution of  
376 profiles failing the check is given in **Fig. S8a, d, g**, indicating a rather uniform temporal and spatial  
377 distribution. A decrease with time of the outlier percentage for OSD data is clearly seen. For CTD  
378 data the outlier percentage is high for all levels and years except for the years after 2020. Argo  
379 profiles failing the check in many cases can be linked to the data from particular floats (**Fig. S8g**).  
380

### 381 **3.8 Local climatological oxygen gradient range check**

382 The oxygen vertical gradient check aims to identify pairs of levels for which the vertical  
383 oxygen gradient exceeds a certain threshold. Threshold values for the vertical gradient (**Fig. 9 g-l**)  
384 are calculated using formula (1), similar to the local oxygen ranges. Due to the nonlinearity of  
385 oxygen profiles, vertical gradient values depend on the profile's vertical resolution, e.g., from the

386 gap between two neighbors' observed levels. Respectively, oxygen thresholds have been calculated  
 387 for several depth gaps between 10m and 100m, as Tan et al. (2023) did for the QC of temperature  
 388 profiles.

389 For level 98 m, the spatial distribution of the oxygen gradient range (Fig. 9i) is similar to the  
 390 spatial pattern of the oxygen range (Fig. 9c), with the largest ranges located in the oxygen minimum  
 391 zones, reflecting the highest oxygen variability in these areas. The region below the main  
 392 thermocline (Fig. 9j-l) is characterized by a much smaller range compared to the 98m level (Fig.  
 393 9g-i). The geographical distribution of profiles failing the check is given in Fig. S9a, d, g,  
 394 indicating a rather uniform temporal and spatial distribution broadly corresponding to the sampling  
 395 density. For CTD data the lowest outlier percentage is observed after 2000 (Fig. S9e).

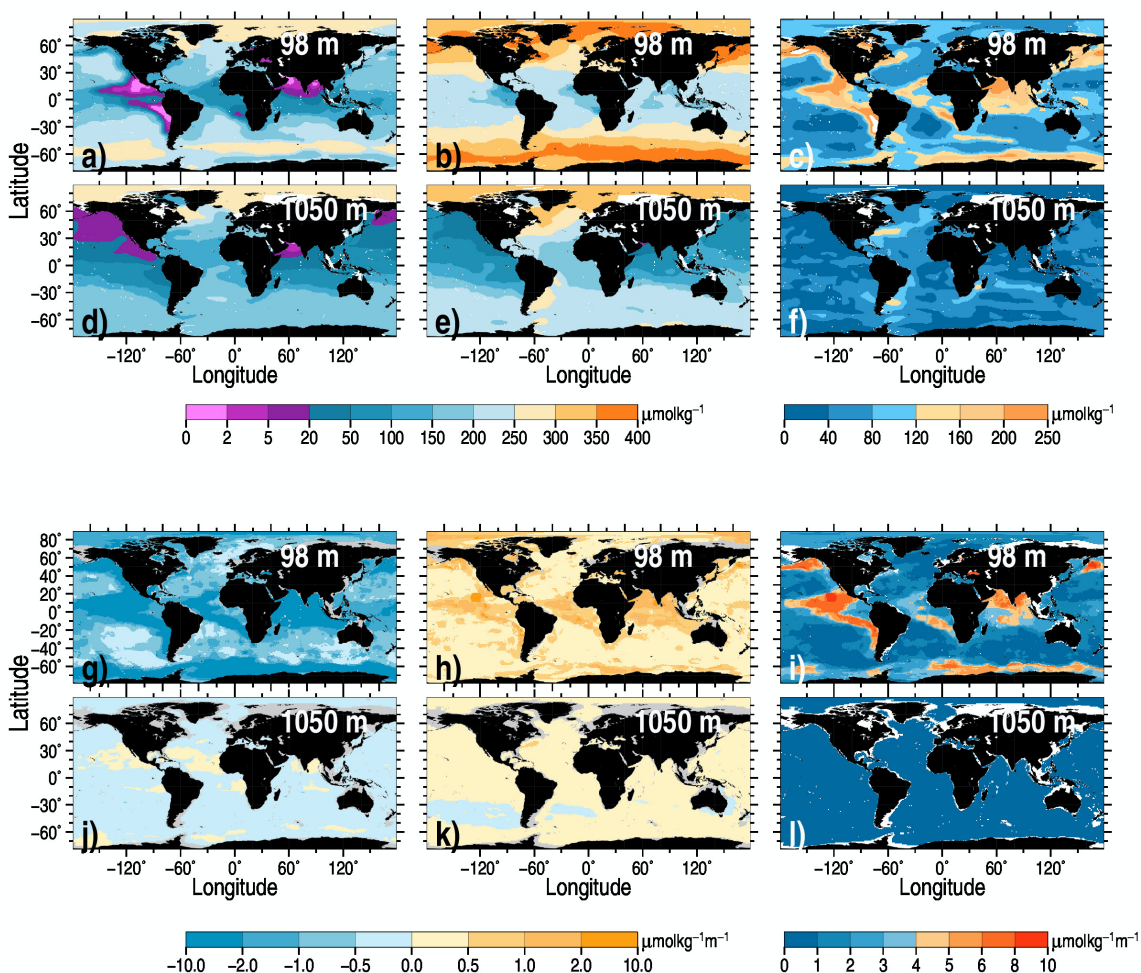


**Figure 9.** Upper six panels: maps of the lower (a), the upper (b) climatological oxygen threshold, and of the oxygen range (c) for the 98m depth level; d-f) same but for the 1050 m depth level. Lower six panels: maps of the lower (g), the upper (h) the climatological oxygen

vertical gradient threshold, and of the oxygen vertical gradient range (i) for 98 m depth level; j-l) same but for the 1050 m depth level.

### 396 3.9 Excessive flagged level percentage check

397 After applying all previous quality checks, the percentage of flagged levels for each oxygen  
398 profile is calculated to produce histograms in **Fig. 10**. A threshold is set based on these histograms  
399 to decide on the quality of the entire profile: we set 20%, 15%, and 30% thresholds for OSD, Argo,  
400 and CTD profiles, respectively. If the threshold is exceeded, the entire profile is flagged, and it is  
401 suggested that it not be used in future analyses. Both the OSD and Argo datasets are characterized  
402 by a low number of profiles with a high percentage of flagged data. In contrast, for the CTD group  
403 the histogram (**Fig. 10c**) exhibits a thick and long tail with a significant fraction of profiles having a  
404 high percentage of flagged levels.

405 The geographical distribution of profiles failing the check is given in **Fig. S10a, d, g**, indicating  
406 a rather uniform temporal and spatial pattern. A decrease of the outlier percentage with time for  
407 OSD data is seen after about 2005 (**Fig. S10b**). For CTD data the outlier percentage is high for all  
408 years except 2021. Argo profiles failing the check in many cases can be linked to distinct floats  
409 (**Fig. S10g**).

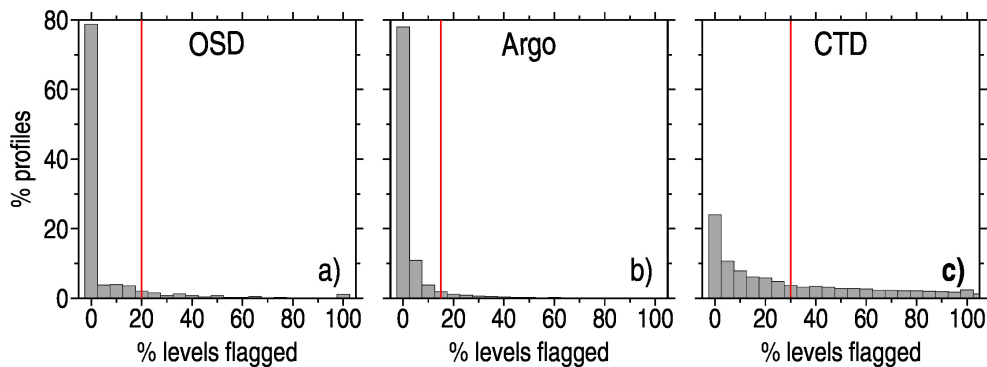
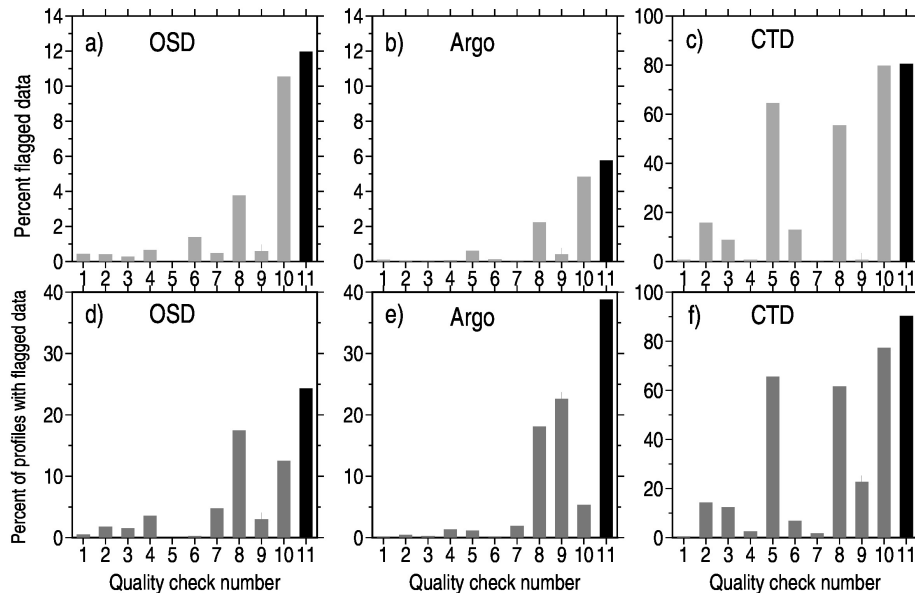


**Figure 10. Percentage of oxygen profiles versus percentage of rejected levels per profile for OSD (a), Argo (b), and CTD (c) instrument types.**

### 410 4 Evaluation of the QC procedure

411 Table 2 and **Figure 11** summarize the rejection rates for all ten quality checks for the three  
412 instrumentation types separately. The Argo oxygen profiles have the lowest overall rejection rate of

413 4.8%, with Winkler data quality ranking second best (12.0% outliers). The difference might likely  
 414 originate from 1) Winkler profiles covering a century-long period of observations, with a poor data  
 415 quality in the earlier decades; 2) the analyzed Argo oxygen data are represented by adjusted  
 416 profiles, which have been already quality-controlled.



417

**Figure 11. (a-c) Percent of measurements flagged by distinct quality checks for three instrumentation types; (d-f) percent of profiles with at least one measurement flagged. For the description of checks see Table 2. The black bar at the number 11 corresponds to the total percent of flagged data (a-c) and to the percent of profiles flagged by at least one quality check (d-f).**

418

419 The CTD oxygen profiles have the highest percentage of outliers (overall rejection rate of  
 420 80.0% for observational measurements). The significant part of CTD oxygen outliers is attributed to  
 421 the stuck value check, which searches for profiles with identical or very similar oxygen values at all  
 422 observed (reported) levels (**Fig. 11a**, check-5). Most of these profiles also fail the local  
 423 climatological range check. We note that these profiles have also been identified as outliers during  
 424 the compilation of the WOA18 (Garcia et al., 2018) and WOA23 (Garcia et al., 2023) atlases of  
 425 dissolved oxygen and have not impacted climatological oxygen distributions presented in these  
 426 atlases.

427

428

As introduced above, the local climatological range check (Check-8 in Table 2) represents the most important quality check and results in the highest percentage of flagged observations and

429 profiles. For OSD, about 17.5% of profiles have at least one measurement flagged by this check.  
430 For Argo and CTD profiles, these values are 18.1% and 61.5%, respectively.

431 **Figure 12** shows the percentage of flagged measurement versus time and depth and within one-  
432 degree latitude/longitude boxes for three main instrumentation types. The OSD group exhibits a  
433 gradual decrease of outlier percentages with time at all depths (**Fig. 12a**), indicating the gradual  
434 improvement of data quality with time, especially after the early 1990s, which coincides with the  
435 beginning of the extensive observational activities during the World Ocean Circulation Experiment  
436 (WOCE). The global spatial pattern of outliers (**Fig. 12b**) is characterized by outlier percentages  
437 lower than 5% in most 1° grid cells, with only a few areas exhibiting higher percentages, which can  
438 be linked to some particular cruises or observational programs.

439 Oxygen data from Argo floats (**Fig. 12c, d**) are characterized by a low percentage of outliers  
440 reflecting the impact of the QC and data adjustments already conducted at DAC centers. We also  
441 find no clear time trend in outlier scores. There is an indication of higher outlier percentages in the  
442 layer below 1500 m before 2020 (**Fig. 12c**). Strong spatial contrasts in the percentage of Argo  
443 outliers (**Fig. 12d**) in most cases can be linked to particular Argo floats.

444 Unlike the OSD Winkler data, CTD oxygen profiles do not suggest a time trend in data quality  
445 (**Fig. 12e**). Compared to both OSD and Argo, ship-based CTD oxygen profiles are characterized by  
446 a much higher outlier percentage. This is explained through a significant fraction of CTD profiles  
447 failing the stuck value check, local climatological range check, and excessive flagged level  
448 percentage check (Table 2). The CTD outlier profiles are evenly distributed over the oceans (**Fig.**  
449 **12f**). **Figure 12g, h** shows outlier distributions for the profiles which passed both the stuck value  
450 and the multiple extrema checks. In this case, most cruise lines (**Fig. 12h**) are characterized by a  
451 low outlier percentage, with data quality issues related to a smaller subset of cruises. Finally, we  
452 find that the CTD data since 2018 (**Fig. 12g**) exhibit very low outlier scores comparable to those of  
453 OSD and Argo float profiles.

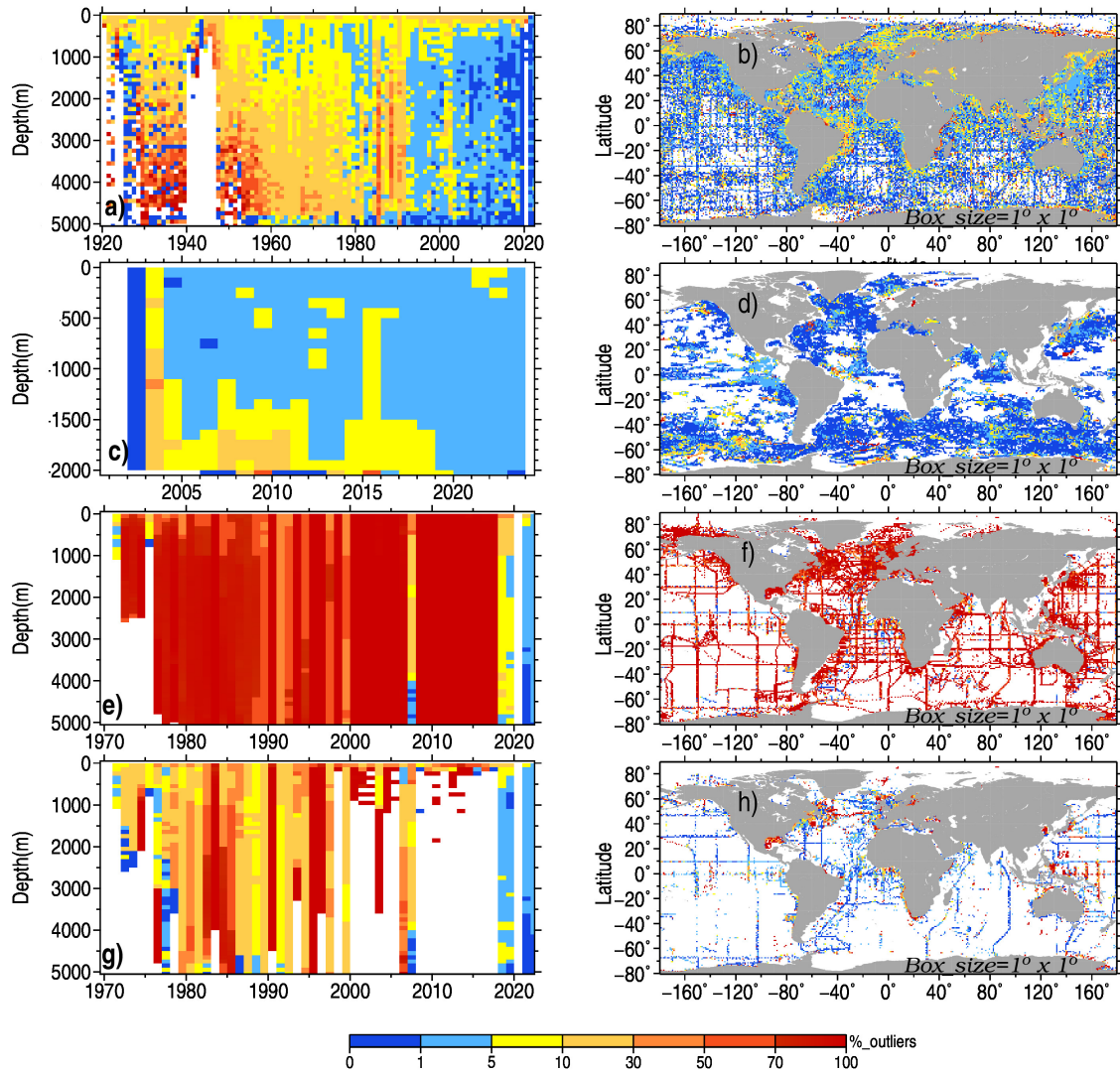


**Figure 12.** Percentage of flagged observations in year/depth bins (a) and in  $1^\circ$  latitude/longitude boxes (b) for OSD oxygen profiles; (c) and (d) same but for Argo oxygen profiles; (e) and (f) same but for CTD oxygen profiles; (g) and (h) same but for CTD oxygen profiles which passed multiple extrema and stuck value quality checks.

454 **Table 2.** Outlier score statistics for different instrumentation types

No.	Quality Check	OSD		CTD		ARGO	
		% flagged observations	% flagged profiles	% flagged observations.	% flagged profiles	% flagged observations	% flagged profiles
1	Location check	0.422	0.478	0.710	0.521	0.086	0.077

2	Global Oxygen Range at depth levels	0.411	1.751	15.797	14.230	0.041	0.421
3	Global Oxygen Range on T surfaces	0.270	1.492	8.824	12.379	0.009	0.227
4	Maximum oxygen solubility check	0.654	3.548	0.638	2.684	0.081	1.325
5	Stuck value check	0.000	00.000	64.547	65.504	0.043	0.073
6	Multiple extrema check	1.376	0.233	12.846	6.802	0.126	0.057
7	Spike check	0.472	4.732	0.039	1.668	0.012	1.904
8	Local climatological oxygen range check	3.766	17.453	55.398	61.513	2.232	18.118
9	Local climatological oxygen vertical gradient range check	0.584	2.962	0.103	6.207	0.181	13.743
10	Excessive flagged level percentage check	10.538	12.489	79.681	76.853	4.434	4.661
	ALL QC CHECKS	11.968	24.564	80.207	84.392	5.191	29.495

455

## 456 **5 Benchmarking of the QC procedure using manually controlled datasets**

457 Evaluation of the QC system is a crucial part of the dataset generation. Good et al. (2022)  
458 conducted a comprehensive benchmarking exercise to evaluate the performance of automated QC  
459 checks for temperature profiles implemented by different research groups, aiming to recommend an  
460 optimal set of quality checks. They used several reference datasets with known quality (e.g., bench-  
461 marking datasets whose quality was manually evaluated by experts).

462 Unfortunately, in a deviation from temperature profiles, no community-agreed oxygen datasets  
463 exist which could be used for benchmarking. In this study, besides the examples of the QC  
464 procedure performance provided for each quality check (Section 3 and Supplementary Material),  
465 we use for the bench-marking a comprehensive set of bottle profile data obtained during the World

466 Ocean Circulation Experiment (WOCE) – the largest international oceanographic experiment ever  
467 conducted (Wunsch, 2005). To achieve high data quality and consistency between the cruises over  
468 the entire period of observations, the WOCE Hydrographic Program Office (WHPO) issued  
469 operation manuals (WHPO, 1991), where measurement methods and procedures are described. As  
470 shown by Gouretski and Jancke, (2000), the WHPO quality requirements have been fulfilled with  
471 the WOCE hydrographic dataset representing a unique global scale high-quality collection of the  
472 whole suite of oceanographic parameters. Specifically, the mean inter-cruise oxygen offset was  
473 found to be  $2.39 \mu\text{mol kg}^{-1}$ . Upon completing the WOCE, the GO-SHIP program was established in  
474 2007 to revise the WOCE hydrographic program by repeating several WOCE lines (Hood et al,  
475 2010).

476 Applying our QC procedure to the entire WOCE dataset confirms the high quality of this  
477 unique dataset, with only 2.8% of oxygen outliers (**Fig. 13a, b**) from the total of 354028 oxygen  
478 measurements for the entire time period 1990-1998. Similar to the entire OSD dataset, the QC  
479 diagnostics reflect the progressive improvement of the oxygen data quality over the period of  
480 WOCE (**Fig. 13a**). The spatial distribution of outliers for the entire time period (**Fig. 13c**) indicates  
481 that the majority of WOCE oxygen profiles have a very low percentage of outliers. For 79% of  
482 WOCE oxygen profiles, our QC procedure identified no data outliers. The higher rejection rate is  
483 found only for several WOCE lines in the tropical South Atlantic, North-Western Indian Ocean, and  
484 the Labrador Sea. We note that, in the same areas, there are data from other cruises which exhibit  
485 low outlier percentages, so the flagging cannot be attributed to the spatial selectivity of the QC  
486 procedure.

487 The WOD database permits data selection for a large number of observational programs using  
488 the respective project identification code. The outlier rejection percentage for the data from 128  
489 projects that reported oxygen data is shown in **Fig. 14**. The mean rejection rate over all projects is  
490 7%. Apart from WOCE, several outstanding observational programs like GEOSECS (Geochemical  
491 Ocean Sections Study) (Craig, 1974), SAVE (South Atlantic Ventilation Experiment) (Larque et al.,  
492 1997), CARINA (Carbon dioxide in the Atlantic Ocean) (Falck and Olsen, 2010), and CLIVAR  
493 (Climate and Ocean: Variability, Predictability and Change) (Sarachick, 1995) delivered a  
494 significant number of high-quality hydrographic data with quality documented in the literature. We  
495 note that the four projects with a median year after 1985 (SAVE, WOCE, CARINA, and CLIVAR)  
496 are characterized by rejection rates lower than the mean. The 8% outlier rate for one of the largest  
497 international GEOSECS experiments conducted in the 1970s only slightly exceeds the mean outlier  
498 percentage over all 128 projects.



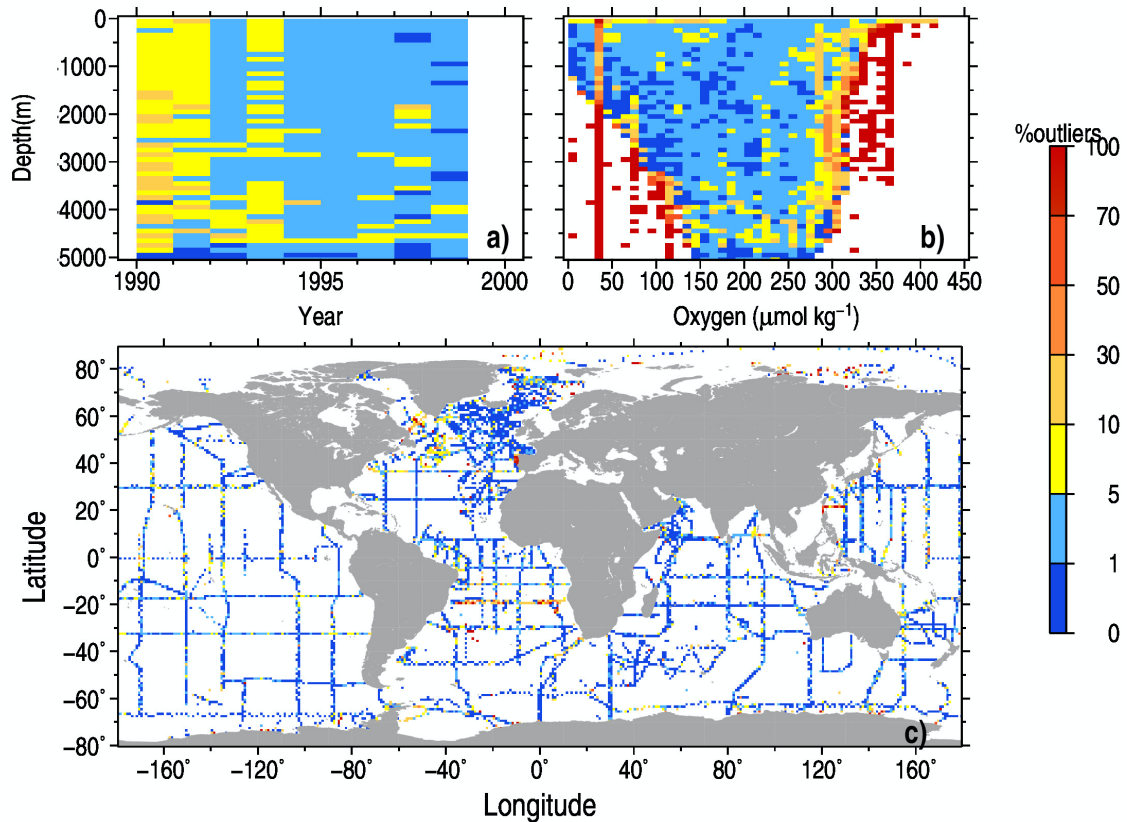
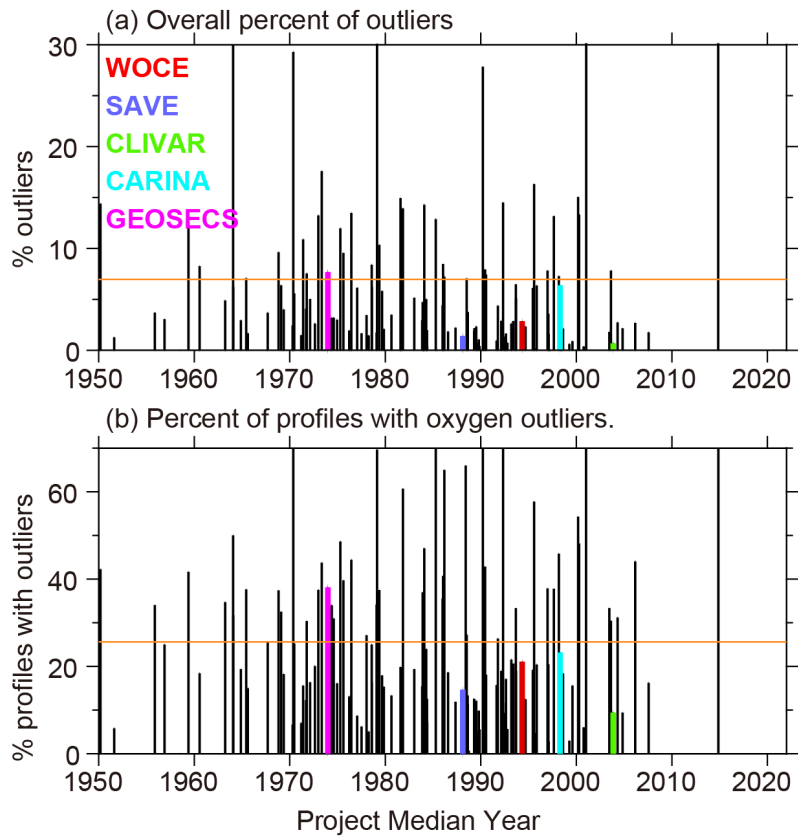


**Figure 13. QC statistics for the WOCE dataset: a) percentage of outliers in year/depth bins; b) percentage of outliers in oxygen/depth bins; c) percentage of outliers in  $1^{\circ}\times 1^{\circ}$  squares.**

500 Finally, we used the delayed mode quality-controlled Argo data to evaluate the performance of  
 501 our QC procedure. The Argo dataset used for the current study consists of oxygen profiles reported  
 502 from 1794 floats. The histogram of the percentage of flagged observations for each Argo float (**Fig.**  
 503 **15a**) shows that for 90% of all floats, the percentage of rejected observations is less than 15%, with  
 504 84% of floats exhibiting less than 5% of rejected measurements. We conclude that the QC applied  
 505 in the DAC centers effectively identifies data outliers for the majority of the floats, resulting in a  
 506 low outlier percentage (see **Fig. 12 c, d**). The location map of profiles from Argo floats with more  
 507 than 15% of data flagged over the float lifetime (**Fig. 15b**) shows a rather random distribution  
 508 throughout the world ocean, with almost all DACs contributing with such floats. We interpreted this  
 509 result as an implicit confirmation of the ability of our QC scheme to identify data with quality  
 510 issues.



511

**Figure 14. Outlier diagnostics for 128 distinct WOD projects (OSD Winkler profiles): a) overall percent of outliers; b) percent of profiles with oxygen outliers. Acronyms and percentages for selected hydrographic projects described in text are shown in color.**

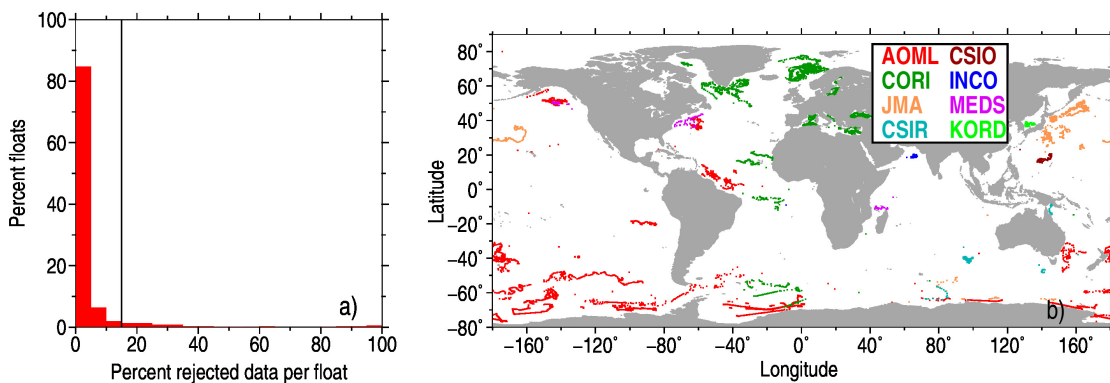


**Figure 15. a) percent of Argo oxygen profiles versus percent of flagged data per profile; b) trajectories of Argo floats with more than 15% of flagged data (a total of 127 floats).**

## 512 6 Bias assessment for sensor oxygen data

513 The QC procedure described in the previous sections is based on the underlying statistics of the  
514 data and aims to identify random outliers. The second step in data QC is estimating the possible  
515 systematic errors or biases. These systematic errors may differ depending on the instrumentation  
516 type, but the common cause for systematic errors is the absence of the possibility to calibrate the  
517 instrument. A classic example provides temperature data obtained by eXpandable  
518 BathyThermographs (XBT) where systematic errors are due to the uncertainty in depth, which is  
519 calculated from the elapsed time, and the uncertainty in thermistor, which is typically not calibrated  
520 (Gouretski and Reseghetti, 2010; Cheng et al., 2014).

521 In the case of dissolved oxygen, only Winkler oxygen determinations of discrete samples can be  
522 considered to be bias-free because the chemical analysis is based on the standard reference, with the  
523 replicate measurements having a precision better than  $0.4 \mu\text{mol kg}^{-1}$  (Thaillandier et al., 2018).  
524 However, differences in methods and standards between hydrographic cruises suggest a lower level  
525 of data precision. Gouretski and Jancke (2000) used the high-quality WOCE one-time hydrographic  
526 dataset and conducted a comprehensive analysis of the inter-cruise oxygen differences at the cruise  
527 cross-over areas. The analysis was performed in the deep part of the water column (typically below  
528 2000 m), where the time variations of seawater properties are small. For 305 cross-over areas, they  
529 estimated the mean difference between WOCE cruises to be  $2.40 \mu\text{mol kg}^{-1}$  with a standard  
530 deviation of  $2.37 \mu\text{mol kg}^{-1}$ . Considering stringent criteria for the WOCE hydrographic program,  
531 this estimate can be considered to represent an approximate precision of the Winkler method in  
532 application to real hydrographic data. As noted by Golterman (1983), the Winkler method still  
533 represents the most precise determination of dissolved oxygen. In spite of some modifications over  
534 time, the principle of the method is unchanged. In the following, we describe residual biases for  
535 CTD and Argo profiles. The term “residual” is used because CTD oxygen profiles are often  
536 adjusted on Winkler bottle samples, and Argo oxygen profiles used in our study undergo adjustment  
537 procedures at the respective DACs.

538 The use of electrochemical and optical oxygen sensors in oceanographic practice has two main  
539 aspects. First, these sensors permitted a significantly higher rate of data acquisition and a much  
540 finer vertical resolution than bottle data. Secondly, they made the observational process much easier  
541 than bottle samples, which need chemical titration in the laboratory. However, like other electronic  
542 sensors, oxygen sensors are prone to offsets and drift. Takeshita et al (2013) analyzed data from 130  
543 Argo floats and found a mean bias of  $-5.0 \%$   $\text{O}_2$  saturation at  $100 \%$   $\text{O}_2$  saturation. Bittig et al.

544 (2018) explained this negative bias by the reduction of O<sub>2</sub> sensitivity proportional to oxygen  
545 content, with the decrease of sensitivity being on the order of several percent per year. Optode drift  
546 characteristics require regular calibration. Use of reference Winkler profiles is possible only for the  
547 ship-based CTD oxygen sensors (mostly electrochemical sensors) if CTD rosette water samples are  
548 obtained simultaneously with sensor profiles and are analyzed for oxygen during a cruise (Uchida et  
549 al., 2010). For unmanned autonomous platforms like Argo, the direct comparison with reference  
550 Winkler data is limited to samples from the hydrographic casts conducted during the float  
551 deployment. Bittig et al. (2018) recommended adjusting optode data on oxygen partial pressure  
552 primarily by the gain (Argo Quality Control Manual, 2021). If no previous delayed-mode  
553 adjustment is available, the basic real-time adjustments are performed based on the oxygen  
554 saturation maps provided by the WOA digital climatological atlas (Thierry et al., 2021). In case a  
555 delayed-mode adjustment is not available after one year, the re-assessment of the gain factor is  
556 recommended. Uncertainty in underlying optode calibration and time drift characteristics leads to  
557 errors in adjusted data.

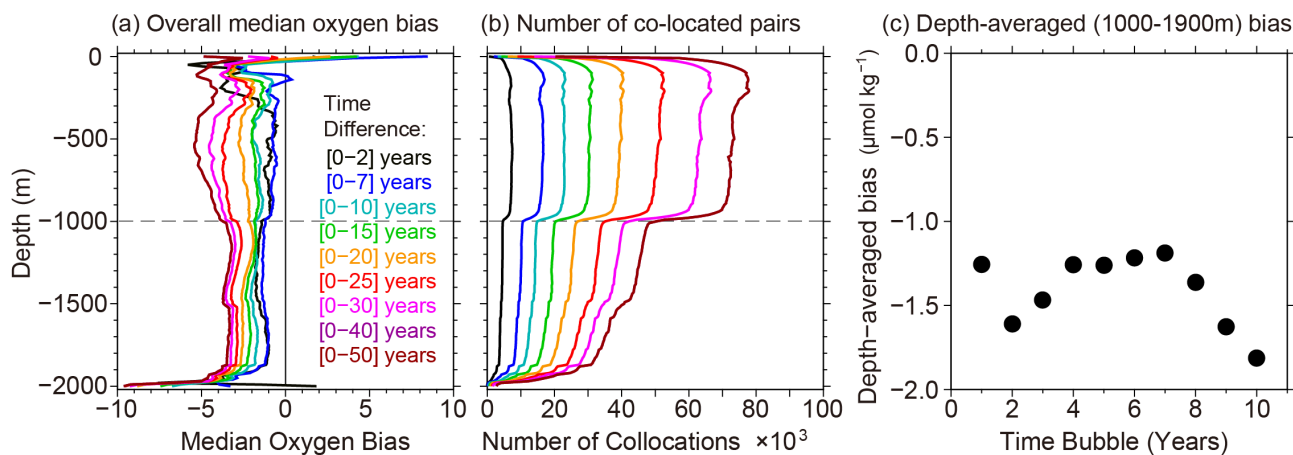
558

## 559 **6.1 Bias assessment method**

560 We aim to assess the magnitude of the possible overall residual bias for CTD profiles and  
561 adjusted Argo profiles by comparing these profiles with collocated reference discrete samples. The  
562 data from 10 national DACs were used for this analysis, for which both unadjusted and adjusted  
563 oxygen profiles are available. Data centers and the respective number of oxygen profiles are given  
564 in Table 1. Data using the Winkler method are used as reference data for the comparison with  
565 collocated Argo oxygen profiles.

566 For the current analysis, we selected a 100 km threshold distance within which two profiles are  
567 spatially collocated. To decide upon the choice of the optimal maximum time difference between  
568 Argo and reference profiles, we calculated median oxygen offsets increasing threshold value for the  
569 time separation between a pair of profiles (**Fig. 16a**). Increasing the temporal collocation bubble  
570 leads to the increase of the bias magnitude in agreement with the assumption that the older  
571 reference data are richer in oxygen compared to the more recent data. Below 1000 m depth, the  
572 difference between the median offsets for the temporal collocation bubble of 5 and 50 years is about  
573 3.5  $\mu\text{mol kg}^{-1}$ , corresponding to a deoxygenation trend of about 0.7  $\mu\text{mol kg}^{-1}$  per decade. This  
574 estimate can be compared with 0.75  $\mu\text{mol kg}^{-1}$  per decade reported by Gregoire et al. (2021). As  
575 **Fig. 16c** suggests, the overall offset estimate below 1000 m stabilizes after the time difference  
576 threshold of 5 years. The extension of the temporal bubble for more than 7 years leads to the

577 progressive increase of the bias magnitude, which we attribute to the impact of the general  
 578 deoxygenation. Based on these calculations, the 5-year threshold was selected as the maximum time  
 579 separation between collocated profiles. For this threshold value, the number of collocated pairs  
 580 below 1000m depth is about 10000 (**Fig. 16b**). A step-wise decrease of the number of collocated  
 581 pairs below 950 m is explained by a significant part of reference profiles being limited to the upper  
 582 1000-meter layer. These calculations suggest that about 1000 collocated pairs are required for stable  
 583 offset estimates.



584

**Figure 16. a) Overall median oxygen bias versus the size of the temporal collocation bubble; b) number of collocated pairs for different choices of collocation bubbles; c) depth-averaged (1000-1900m) bias versus time bubble size.**

585

586 The number of Argo profiles having collocations with discrete ship-based Winkler profiles is  
 587 shown in Table 1. No collocated Winkler profiles are found for the Argo profiles from the two  
 588 Korean DACs. Profiles from these DACs are restricted within a relatively small area east of the  
 589 Korean peninsula. The four largest contributors of Argo data (AOML, Coriolis, JMA, and CSIRO)  
 590 comprise up to 90% of all Argo profiles having collocations with reference profiles.

591

## 592 6.2 Overall bias characteristics of unadjusted and adjusted Argo oxygen data from DACS

593 The normalized frequency histograms (**Fig. 17**) characterize the spread of individual bias  
 594 estimates around the distribution mode. These histograms are based on all Argo profiles having  
 595 collocations with reference Winkler data. In these histograms, for each depth bin, the number of  
 596 values in each bias bin is normalized by the number for the most populated bias bin at each depth  
 597 level to account for the decrease of data with depth. The histograms are shown for raw (unadjusted)  
 598 (**Fig. 17a**) and adjusted Argo profiles (**Fig. 17b**). The adjustment procedures applied at different

599 DACs reduce the spread of the individual bias estimates and the skewness of the bias distribution,  
 600 with the overall median bias of 10-12  $\mu\text{mol kg}^{-1}$  for unadjusted data and 1-2  $\mu\text{mol kg}^{-1}$  for adjusted  
 601 data. As suggested by the bias distribution with depth, we estimate residual bias using the collocated  
 602 data below 1000 m depth, where the bias spread reduces significantly compared to the upper part of  
 603 the water column.  
 604

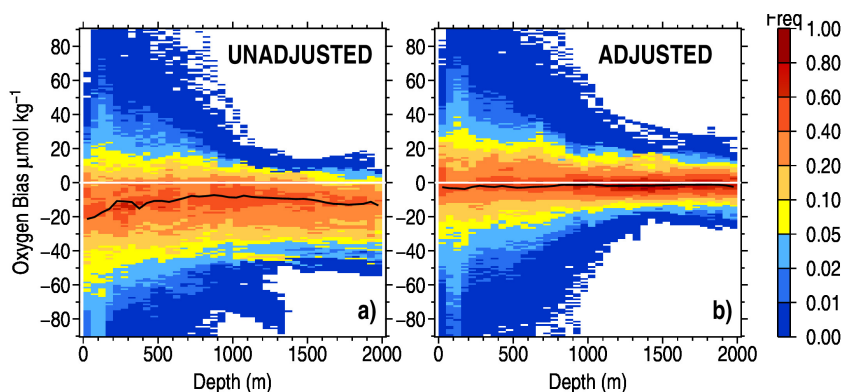


**Figure 17. Normalized histograms of the unadjusted (a) and adjusted (b) Argo oxygen bias versus collocated Winkler profiles. The black lines show the median bias value.**

605

### 606 6.3 Residual Oxygen Biases for distinct oxygen sensor

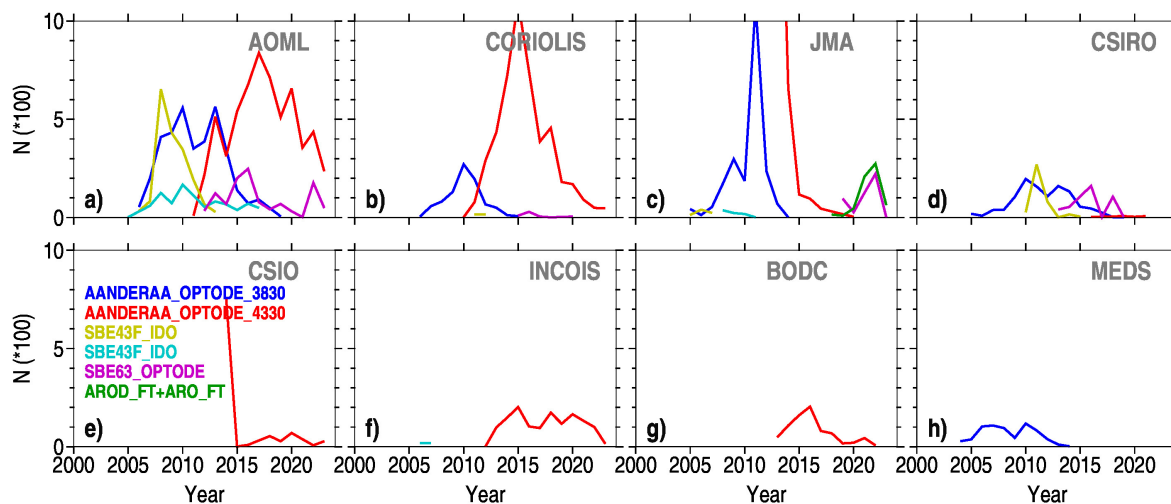
607 A total of 11 oxygen sensor models were implemented on Argo BGC floats, with 8 sensor  
 608 models found among Argo profiles having collocations with reference data (see Table 3). **Figure 18**  
 609 shows the yearly number of Argo profiles that have collocations with reference data and are  
 610 equipped with different models of oxygen sensors. The SBE43 series sensors are electrochemical  
 611 Clark-type sensors, whereas all other models are optical sensors (optodes). Since the beginning of  
 612 the 2000s, several models of optodes have been implemented in BGC Argo floats. The two most  
 613 widespread sensors are AANDERAA 3830, implemented between 2004 and 2018, and the newer  
 614 model AANDERAA 4330 used since 2010. The majority of Argo floats from the three largest  
 615 AOML, Coriolis, and JMA datasets have been equipped with this sensor. Data from AOML,  
 616 Coriolis, JMA, and CSIRO include oxygen profiles obtained by means of several sensor models.  
 617 The other four DAC subsets of data are represented by a single sensor model:  
 618 AANDERAA\_OPTODE\_4330 prevails in the data from INCOIS, CSIO, and BODC, and

619 AANDERAA\_OPTODE\_3830 is typical for MEDS data. AROD\_FT and ARO\_FT optodes have  
 620 been implemented only on Argo floats managed by JMA.

621

622 **Table 3. Oxygen sensors installed on BGC Argo floats**

N	Oxygen Sensor Model	Number of Argo profiles	Number of Argo profiles collocated with Winkler profiles
<b>Optode sensors</b>			
1	AANDERAA_OPTODE_4330	160261	16112
2	AANDERAA_OPTODE_3830	49049	8234
3	AANDERAA_OPTODE_3835	405	0
4	AANDERAA_OPTODE_4831	454	0
5	SBE63_OPTODE	16775	1978
6	SBE83_OPTODE	462	0
7	ARO_FT	2792	618
8	AROD_FT	370	31
<b>Clarke-type sensors</b>			
9	SBE43F_IDO	12234	2341
10	SBE43I	9620	1046
11	SBE43_IDO	2173	246



624 **Figure 18. Yearly number of BGC Argo profiles equipped with different types of oxygen**  
 625 **sensors (colored lines, see sensor attribution in plate e)). (a) AOML, (b) Coriolis, (c) JMA, and**  
 626 **(d) CSIRO, e) CSIO, f) INCOIS, g) BODC, h) MEDS.**

627 According to the Argo Quality Control Manual (Thierry et al., 2021), several adjustment  
 628 procedures can be applied to unadjusted data (adjustment to climatology, nearby Winkler samples,  
 629 or in-air data). The adjustment results may depend on many factors, such as the subjective decision  
 630 of the operator in a DAC, the use of a specific software, the availability of the respective reference  
 631 data, and other factors. If a climatology is used as a reference, the Argo oxygen values will be  
 632 adjusted to the median year of a climatology, which can differ by several decades from the year of  
 633 an Argo profile. In such cases, the long-term deoxygenation trend of the world ocean might impact  
 634 the results of the adjustment procedure. Differences in the applied adjustment procedures may  
 635 potentially result in DAC-specific residual offsets. Considering these two main causes for biases in  
 636 sensor oxygen data, we calculated profiles of overall oxygen biases versus depth (e.g. biases based  
 637 on the data from all years) for six sensor models (1, 2, 5, 6, 8, and 10, see Table 3) and for six DACs  
 638 which provided a sufficient number of collocated pairs (**Fig. 19**).

639 The number of available collocations with reference Winkler profiles varies by two orders of  
 640 magnitude for different DACs. Since reference bottle data often cover only part of the upper 2000-  
 641 meter layer, the number of collocated pairs also changes over depth, with the main step-wise  
 642 decrease seen around 1000 m. However, our calculations suggest that changes in the number of  
 643 collocated pairs over depth do not significantly impact the diagnosed bias. In order to reduce the  
 644 effect of the varying geographical sampling pattern over depth, only Argo profiles deeper than 1000



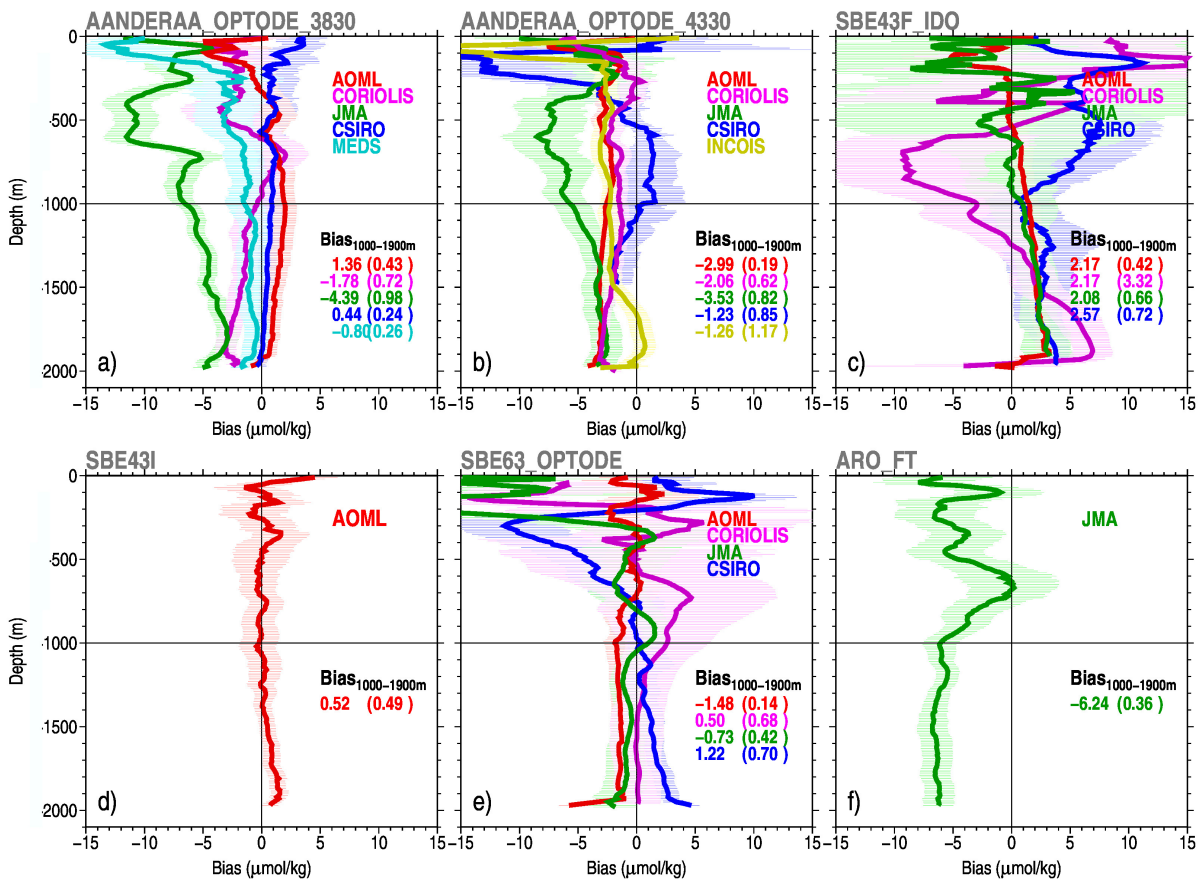
645 m were used for bias calculations. **Figure 19** shows a much higher variability of diagnosed biases in  
646 the upper part of the water column due to a stronger temporal and spatial oxygen variability.  
647 However, in the layer below 1000 m (e.g., crudely below the main thermocline), all profiles indicate  
648 much smaller variations over depth, and in the following discussion, we will focus on biases within  
649 this layer.

650 For almost all oxygen sensors, the overall bias exhibits a characteristic hook below about 1900-  
651 1950 meters. Such hooks on Argo oxygen profiles were found by Thallander et al., (2018). The  
652 hook can reflect the adjustment of the oxygen sensor at the beginning of the float ascending. Further  
653 we note that Clarke-type sensors from SBE43 series are characterized by a positive oxygen bias  
654 below 1000 m, whereas the majority of optodes is characterized by negative biases, with the  
655 exception of SBE63 profiles in CSIRO data.

656 Another feature common to AANDERAA optodes and SBE43-series sensors is the dependence  
657 of bias on depth (pressure). For one and the same sensor model, the slope of the bias profile differs  
658 among the DACs. The most clear dependence on pressure is seen for the SBE43F IDO and SBE43I  
659 models for AOML data (**Fig. 19c, d**) and for AANDERAA\_3830\_OPTODE for the four largest  
660 DAC datasets (**Fig. 19a**). It is known that dissolved oxygen measurements by SBE43-IDO series  
661 sensors are influenced by changes of sensor membrane characteristics due to temperature and  
662 pressure. Depending on the sensor's time-pressure history, these changes have long time constants,  
663 resulting in hysteresis at depths greater than 1000 meters (Thierry et al., 2021). Until now, there has  
664 been no effective method for adjusting the pressure effects of these sensors on profiling floats under  
665 operation. Data from all optodes also require adjustments for pressure effects (Bittig et al., 2015).  
666 Increasing pressure reduces the oxygen concentration inside the sensing membrane (which is  
667 relevant for luminescence quenching) by ca. 3.0 - 5.5% per 1000 dbar. The optodes are thus  
668 expected to show lower oxygen under pressure, which is confirmed by our **Fig. 19a, b** for all DACs  
669 except JMA.

670 Also shown in **Fig. 19** are estimates of mean biases calculated for the layer 1000-1900m ( $B_{1000-}$   
671  $1900m$ ). The lower boundary of 1900m was selected in order to exclude the depth range where bias  
672 profiles exhibit characteristic hooks described above. In order to assess the stability of the overall  
673 biases shown in **Fig. 19**, we calculated the time series of the bias for the layer 1000-1900m for six  
674 most numerous sensor models (**Fig. 20**). The changes of the diagnosed biases over time indicate a  
675 certain degree of sensor stability with biases typically retaining the same sign throughout the entire  
676 period of observations. We attribute at least a part of this layer's apparent bias time variability to the  
677 changes in the geographical sampling and the differences in the reference data.

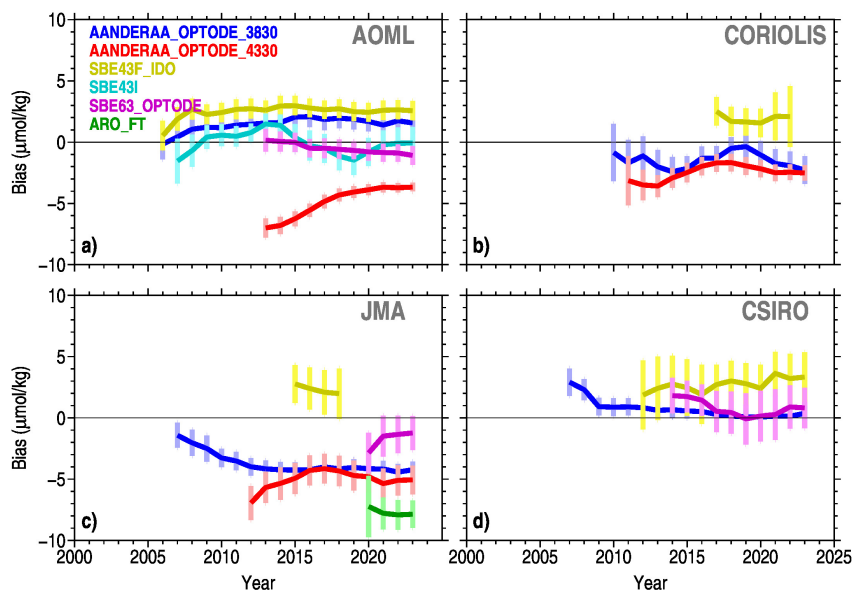
678



679 **Figure 19. Overall oxygen biases for six oxygen sensor models: a)**  
 680 **AANDERAA\_OPTODE\_3830, b) AANDERAA\_OPTODE\_4330, c) SBE43F\_IDO, d) SBE43I,**  
 681 **e) SBE63\_OPTODE, f) ARO\_FT. Bias profiles are shown for the six largest DAC datasets**  
 682 **(colour lines). Values of the average bias for the layer 1000-1900m ( $B_{1000-1900\text{m}}$ ) are shown in**  
 683 **the lower right part of each panel, with standard errors given in parentheses. Light colour**

684 shading corresponds to the bias standard error at depth levels with the number of degrees of  
685 freedom equal to the number of distinct Argo floats.

686



687 **Figure 20. Residual oxygen bias for the layer 1000-1900m versus time. Vertical bars show**  
688 **standard error with the number of degrees of freedom equal to the number of distinct floats.**  
689 **Each value corresponds to the bias averaged within the five-year time window. Calculations**  
690 **are shown for the data from distinct DACs: a) AOML, b) Coriolis, c) JMA, d) CSIRO.**

691

692 In order to assess the stability of the overall bias estimates shown in **Fig. 19**, we calculated  
693 time series of the average bias within the layer 1000-1900m for six most abundant sensor models  
694 (**Fig. 20**). The changes of the diagnosed biases over time indicate a certain degree of sensor stability  
695 with biases typically remaining positive or negative over the entire period of observations. At least  
696 part of this apparent time variability may be due to the changes in the number of collocated pairs  
697 and their geographical distribution over time. Considering the strong limitation imposed by the  
698 number of available collocated pairs, we suggest overall constant bias corrections for different  
699 sensors and DACs (Table 4). These corrections correspond to the residual biases in the layer 1000-  
700 1900 m (see **Fig. 19**).

701

702 **Table 4. Sensor-specific bias corrections for data from different DACs<sup>\*)</sup>**

703

704

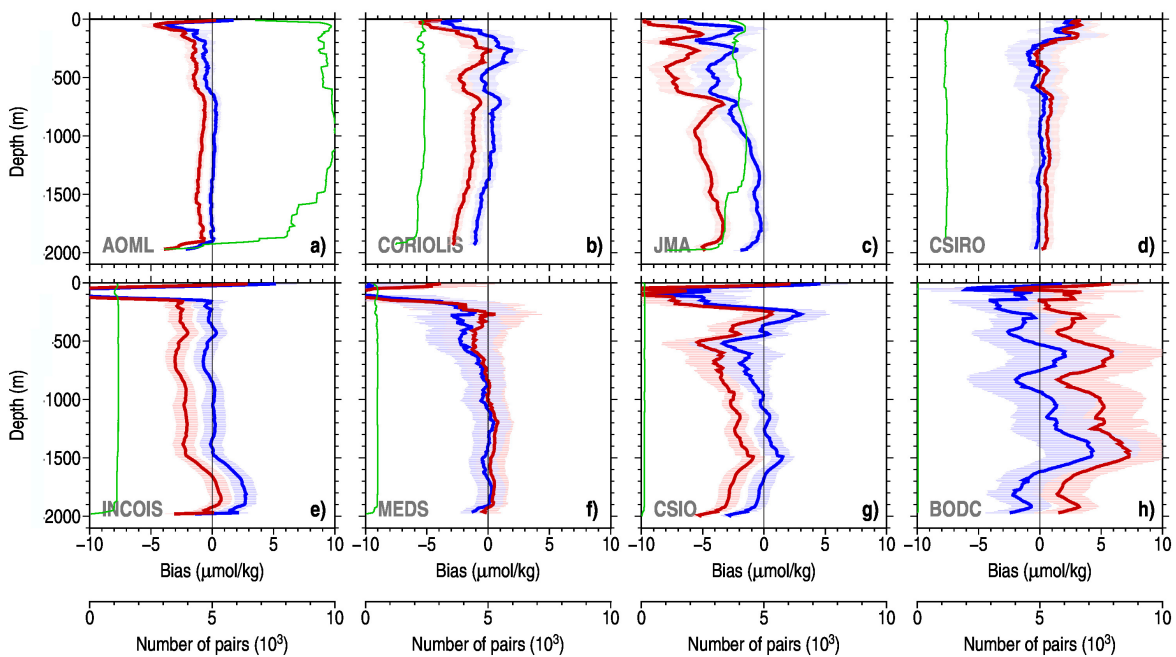
	Sensor model	AANDERAA_ OPTODE_383 0	AANDERAA_ OPTODE_433 0	AROD_FT, ARO_FT	SBE43F_I DO	SBE43I	SBE63_OPTO DE
1	<b>AOML</b>	1.36(0.43)	-3.22(0.19)		2.17(0.42)	0.52(0.42)	-1.07(0.16)
2	<b>Coriolis</b>	-1.78(0.72)	-2.06(0.62)		2.17(3.32)		0.50(0.68)
3	<b>JMA</b>	4.38(0.99)	-3.19(0.52)	-6.24(0.36)	2.08(0.67)	0.52	-0.74(0.42)
4	<b>CSIRO</b>	0.44(0.24)	-1.23(0.70)		2.57(0.72)		1.22(0.70)
5	<b>CSIO</b>		-2.43				-0.02
6	<b>INCOIS</b>		-2.43			0.52	
7	<b>BODC</b>		4.00(2.07)				
8	<b>MEDS</b>	-1.09	-2.43				-0.02
9	<b>KORD</b>	1.09			2.25		
10	<b>KMA</b>		-2.43				

705 \*) Bias corrections are given in  $\mu\text{mol/kg}$ . Values in parentheses show standard errors. If standard  
706 error is not shown the correction indicates a guess value equal to the mean of values with standard  
707 error estimate. Corrections indicated in the table should be subtracted from the reported oxygen  
708 value. Empty boxes correspond to the sensors which are absent for a specific DAC.

709

710 Finally, overall biases were calculated for the data from eight distinct DACs (Korean datasets  
711 from KORDI and KMA are relatively small and do not have collocations with reference cruises  
712 available for this study). Biases were calculated for the original data (QC-ed and adjusted by DACs)  
713 and for the data corrected for residual biases according to Table 4 (**Fig. 21**). For all DACs, the  
714 suggested bias corrections led to the reduction of the overall bias. AOML, CSIRO, and MEDS data

715 are characterized by a rather constant bias below about 700 m depth. Bias profiles for Coriolis and  
 716 JMA subsets of data indicate the possible impact of pressure effect on oxygen sensors discussed  
 717 above. It should be noted that the number of collocated profile pairs differs by two orders of  
 718 magnitude among the eight DACs. In the layer above 1900 m, the AOML data has between 6500-  
 719 9500 collocated pairs for each depth level, whereas the BODC dataset contributes only with 37  
 720 Argo profiles having collocations with reference data. A larger variability of the bias over depth for  
 721 CSIO and BODC data is most likely explained by the insufficient sample size.  
 722



723  
 724 **Figure 21. Overall mean Argo oxygen offsets versus Winkler profiles for distinct DACs: a)**  
 725 **AOML, b) Coriolis, c) JMA, d) CSIRO, e) INCOIS, f) MEDS, g) CSIO, h) BODC. Offset**  
 726 **profiles for DAC-adjusted data and for the data corrected for residual biases (Table 4) are**  
 727 **shown in red and blue, respectively. Standard error bars (light shading) are calculated using**  
 728 **the number of distinct floats at each level as the number of degrees of freedom. Green lines**  
 729 **show number of collocated pairs in thousands.**

730

#### 731 6.4 Residual Oxygen Biases for CTD oxygen sensors

732 We conducted similar bias calculations for the CTD oxygen profiles obtained by both  
 733 electrochemical and optical sensors. Only CTD data which passed all QC checks were used for the  
 734 bias estimation. Unlike Argo profiles, the CTD oxygen sensor data can be adjusted on the  
 735 simultaneously collected bottles analyzed in the ship laboratory using the Winkler method

736 (Taillandier et al., 2018). Unfortunately, it is not possible to identify profiles with such adjustments  
737 within the WOD archive because of missing metadata. As noted by Boyer et al. (2018) “in many  
738 cases, the dissolved oxygen ... data are uncalibrated and not of high quality. Information on  
739 whether these variables are calibrated is not usually supplied by the data submitter”. As noted by  
740 Uchida et al. (2010) calibration of oxygen sensor profiles is not straightforward, requires some  
741 expertise, and depends on the quality of the reference data. Saout-Grit et al. (2015) described the  
742 calibration procedure for SBE-43 sensor done by fitting to reference Winkler data and found a time  
743 trend in residuals during the analyzed cruise. WOD archives the data submitted by the data  
744 producers and other resources. Thus, the data quality and calibration procedure of the CTD oxygen  
745 data are likely inhomogeneous.

746 For 0-1900 m, we find an overall CTD oxygen offset of about  $0.25 \mu\text{mol kg}^{-1}$  (median) relative  
747 to the Winkler data over the 1960-2022 period, which is much smaller than Argo oxygen biases  
748 ranging from  $-3.72$  (JMA) to  $0.76 \mu\text{mol kg}^{-1}$  (CSIRO) (see **Fig. 19**). Similar to Argo data the offset  
749 distribution above 1000 m level (**Fig. 22e**) exhibits stronger spread than that below 1000 m. The  
750 median offset for the layer 1000-2000 m is  $0.25 \mu\text{mol kg}^{-1}$ . Grégoire et al. (2021) indicated that  
751 “*the uncertainty associated with the last generation of  $O_2$  sensors that uses the best calibration and*  
752 *calculation methods amounts, in the best case at  $\sim 2 \mu\text{mol kg}^{-1}$ ””. Therefore, the overall median  
753 offset of  $0.25 \mu\text{mol kg}^{-1}$  identified by this study is well within the expected uncertainty of the CTD  
754 sensors. Besides, there is no spatial uniform pattern for the CTD offsets (**Fig. 22d**), implying that  
755 this offset might not be systematic. Further investigation of the offsets for different cruises (figure  
756 not shown) indicates that the offset varies cruise by cruise and year by year. Therefore, in this  
757 study, we decided not to adjust the CTD data before the offset can be further confirmed after a  
758 cruise-by-cruise investigation, and the underlying reasons for the bias can be understood.*

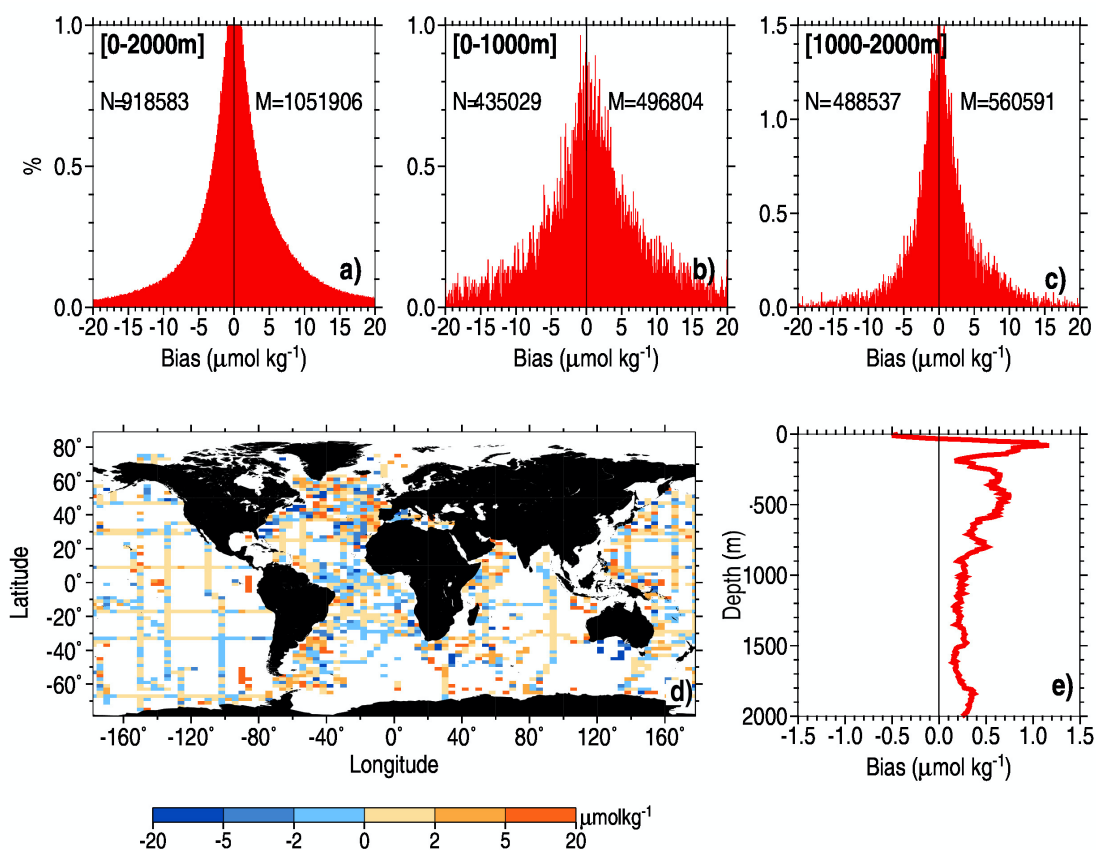


**Figure 22. Statistics of the CTD oxygen bias relative to co-located Winkler data. Histograms of layer-averaged bias for 0-2000 m (a), 0-1000 m (b) and 1000-2000 m (c). Number of negative (N) and positive (M) bias values is shown respectively on the left and right side of each histogram. (d) median of depth-averaged bias (1000-2000m) in  $2^{\circ} \times 4^{\circ}$  grid boxes; (e) overall median CTD oxygen offset as a function of depth.**

760

## 761 7. Impact of quality control and bias adjustment on estimating oxygen changes

762 Applying the QC and bias adjustment to historical *in situ* oxygen data is expected to impact the  
 763 derived ocean oxygen changes on various spatial/temporal scales. To illustrate this impact, we  
 764 implemented the new Auto-QC system for all oxygen data and adjusted the Argo data based on the  
 765 approach described in Section 6. Based on these data, we applied the mapping method (Ensemble  
 766 Optimal Interpolation approach with a Dynamic Ensemble from climate model simulations, EnOI-  
 767 DE) proposed by Cheng et al. (2017, 2020) to spatially interpolate oxygen data, yielding a spatially  
 768 complete gridded global ocean oxygen dataset. Because of the limited spatial coverage of oxygen  
 769 data, we combine each successive three years of data to derive oxygen fields for each calendar year.

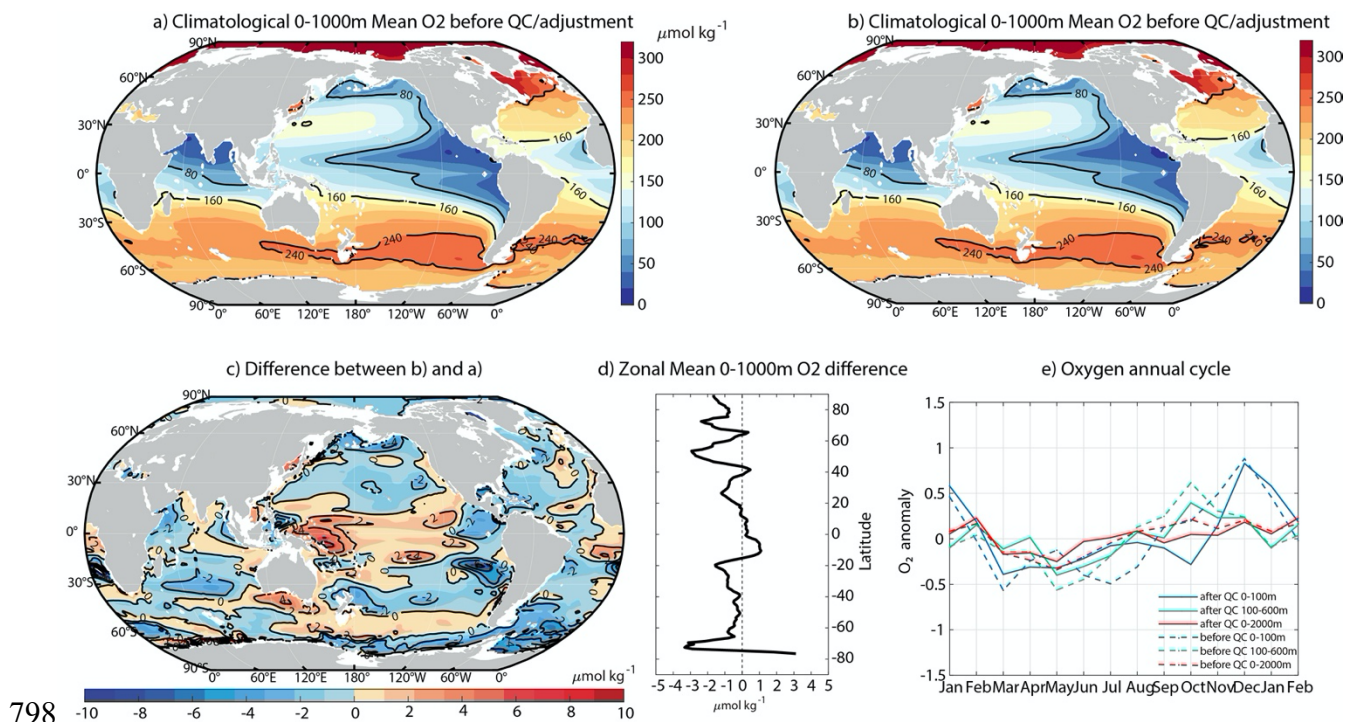
770 Respectively, the oxygen time series are based on these fields. The reconstruction is only done for  
771 the upper 2000 m because of the insufficient in situ data in the abyssal layers. The resultant oxygen  
772 field is denoted as “after QC/adjustment”. To show the impact of QC and adjustment on the oxygen  
773 changes estimate, we also applied the same method to the data without QC (e.g. with only several  
774 crude QC checks applied to remove most likely erroneous values, including overall range checks,  
775 solubility check, and spike check) and without Argo adjustments. The resultant field is denoted as  
776 “before QC/adjustment”.

777 The long-term mean states (e.g., the climatology, reconstructed using all data between 1990-  
778 2022 based on EnOI-DE approach) of the upper 1000 m oxygen before and after QC/adjustment are  
779 very similar (**Figs. 23a, b**). One reason is the EnOI-DE method (as any mapping approach) has a  
780 smoothing effect, so the erroneous data is less visible behind high spatial variability. This indicates  
781 the robust large-scale pattern, where the oceans in the low latitudes have lower oxygen  
782 concentrations than in the higher latitudes because of the water temperature and ocean circulation  
783 difference. The Eastern Pacific and North Indian Oceans show even lower oxygen levels because of  
784 the subsurface oxygen minimum zone. The difference between oxygen climatologies calculated  
785 before and after QC/adjustment ranges from  $-15\sim 15\ \mu\text{mol kg}^{-1}$  but differs at different locations (**Fig.**  
786 **23c**). The zonal mean difference is smaller ( $-3\sim 1\ \mu\text{mol kg}^{-1}$ ) because of the error cancellation at  
787 each latitude (**Fig. 23d**).

788 The QC/adjustment also impacts the annual cycle (including both phase and magnitude) of the  
789 global mean oxygen changes (**Fig. 23e**). Examples for the layers 0 – 100 m (representing the upper  
790 seasonal change layer), 100 – 600 m (representing the main thermocline) and 0 – 2000 m (showing  
791 the ocean oxygen inventory) are shown in **Fig. 23e**. For 0 – 100 m, the mean oxygen level shifts  
792 from negative to positive in November after QC/adjustment but in September before  
793 QC/adjustment. The magnitude of the annual cycle, if simply defined as the difference between the  
794 maximum and minimum of the 12-month climatology time series, is  $1.45\ \mu\text{mol kg}^{-1}$  but slightly  
795 reduced after QC/adjustment ( $1.22\ \mu\text{mol kg}^{-1}$ ). The magnitude of the 100 – 600 m and 0 – 2000 m



796 annual cycle has also been reduced after QC/adjustment (1.18, 0.55  $\mu\text{mol kg}^{-1}$  before  
 797 QC/adjustment and 0.79, 0.48  $\mu\text{mol kg}^{-1}$  for 100 – 600 m and 0 – 2000 m, respectively, **Fig. 23e**).

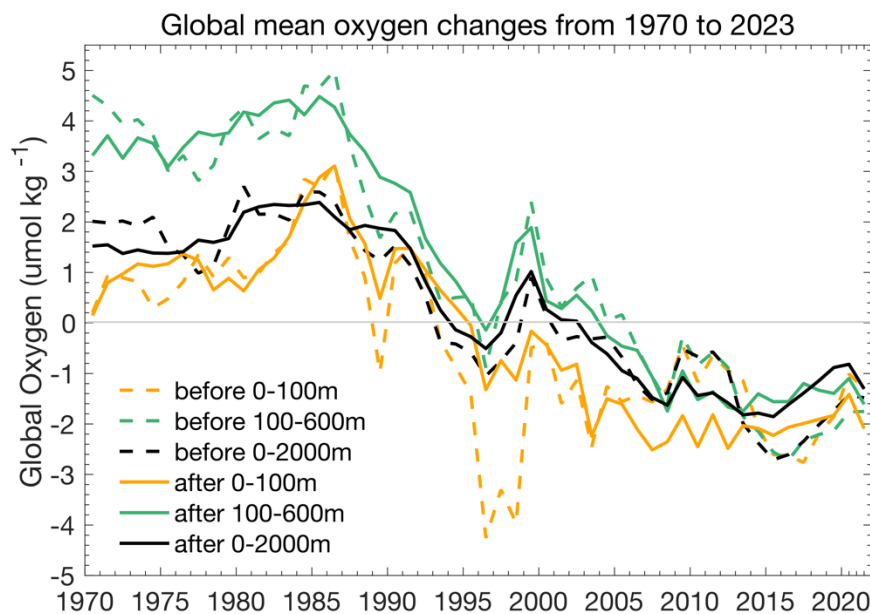


798 **Figure 23. The climatological upper 1000 m oxygen field before (a) and after (b)**  
 799 **QC/adjustment, with their spatial difference shown in (c) and zonal mean differences in (d).**  
 800 **The annual cycle (relative to the climatological annual mean level) before (dashed line) and**  
 801 **after (solid line) QC/adjustment are compared in (e) for different vertical layers. The**  
 802 **climatology field is reconstructed by combining all data within 1990-2022 with EnOI-DE**  
 803 **mapping method (Cheng et al. 2017, 2020).**  
 804

805  
 806 The QC and adjustment also impact the estimates of long-term oxygen changes, for example  
 807 the global deoxygenation estimates for 0 – 100 m, 100 – 600 m and 0 – 2000 m layers depicted in  
 808 **Fig. 24**. After QC/adjustment, the standard deviation of the time series is decreased from 1.71 (0 –  
 809 100m), 2.37 (100 – 600m), 1.60 (0 – 2000m) to 1.62 (0 – 100m), 2.24 (100 – 600m), 1.44 (0 –  
 810 2000m)  $\mu\text{mol kg}^{-1}$ , showing a reduced variability in global oxygen time series after QC/adjustment.  
 811 This indicates a reduction of noise, which is mainly attributed to both QC and Argo adjustment. For  
 812 example, before QC/adjustment, there was a big global 0-100m deoxygenation of  $\sim 3 \mu\text{mol kg}^{-1}$   
 813 from 1995 to 1996, which is likely non-physical and spurious. Such change disappeared after  
 814 QC/adjustment (**Fig. 24**). The linear rate of deoxygenation differs for the two tests as well:  $-0.77 \pm$

815  $0.43$  ( $0 - 100\text{m}$ ),  $-1.45 \pm 0.30$  ( $100 - 600\text{m}$ ),  $-0.95 \pm 0.30$  ( $0 - 2000\text{m}$ )  $\mu\text{mol kg}^{-1} \text{dec}^{-1}$  before  
 816 QC/adjustment and  $-0.90 \pm 0.38$  ( $0 - 100\text{m}$ ),  $-1.37 \pm 0.40$  ( $100 - 600\text{m}$ ),  $-0.84 \pm 0.41$  ( $0 - 2000\text{m}$ )  
 817  $\mu\text{mol kg}^{-1} \text{dec}^{-1}$  after QC/adjustment. The linear trend is calculated by the ordinary least square  
 818 regression with a 90% confidence interval shown (accounting for the reduction in degree of  
 819 freedom). The deoxygenation rates are reduced after QC/adjustment for both  $100 - 600\text{m}$  and  $0 -$   
 820  $2000\text{m}$ , mainly because of the Argo adjustment, which shifted the oxygen level in the past decade  
 821 by  $\sim 0.76 \mu\text{mol kg}^{-1}$  for  $100 - 600 \text{ m}$  average and  $\sim 0.82 \mu\text{mol kg}^{-1}$  for  $0 - 2000 \text{ m}$  average within  
 822 2015-2023 (**Fig. 24**).

823 By means of these tests we demonstrate that QC and bias adjustment can impact the estimation  
 824 of the oxygen changes at various temporal-spatial scales, highlighting the need for careful oxygen  
 825 data processing before application. However, we note here that the validity of the mapping  
 826 approach on oxygen reconstruction has not been thoroughly evaluated, which deserves a separate  
 827 study.



828  
 829 **Figure 24. The reconstructed global averaged oxygen time series before (dashed line) and**  
 830 **after (solid line) QC/adjustment from 1970 to 2023 for the layers  $0 - 100 \text{ m}$ ,  $100 - 600 \text{ m}$  and**

831 **0 – 2000 m. Here, we combine each successive three years of data to estimate the oxygen**  
832 **changes. The anomalies are calculated relative to the climatology shown in Fig. 23.**

833

## 834 **8 Conclusion and Discussion**

835 This study developed a new automated QC scheme for ocean oxygen profile data and applied it  
836 to the OSD and CTD oxygen profiles from the WOD and to the Argo float oxygen profiles provided  
837 by national DACs. The procedure consists of ten quality checks based on local or global parameter  
838 thresholds. Some checks are conceptually similar to the quality checks used to validate the profiles  
839 in the World Ocean Database (Boyer et al., 2018) (for example, the global range test and vertical  
840 gradient test) and in the Argo data acquisition centers (Thierry et al., 2021) (for example, spike and  
841 “frozen” profile tests). However we provide additional checks (for example, test for the number of  
842 local extrema and local climatological range test) which increase the ability of the QC procedure to  
843 better identify erroneous data. For instance, the procedure proves whether an oxygen value falls out  
844 of accepted ranges (defined by globally or locally) or whether an oxygen profile exhibits a very  
845 untypical shape. The shape of the profile is characterized by the vertical oxygen gradient, the  
846 number and magnitude of local oxygen extrema, and by the presence of spikes. The check is also  
847 done for the so-called “frozen” profiles occurring when the oxygen sensor sticks and reports the  
848 same values throughout the profile.

849 The QC procedure presented here is tailored for the quality assessment of the archived oxygen  
850 data obtained both by Winkler methods and sensors. Large ocean depositories like WOD often  
851 contain observed data that have already undergone a certain degree of QC and adjustment.  
852 Therefore, our QC procedure differs from the real-time QC of dissolved oxygen observations by  
853 means of oxygen sensors as suggested in the frame of the Integrated Ocean Observing System  
854 (IOOS) in the quality control manual by Bushnell et al. (2015) (B2015 hereafter). Three quality  
855 tests which have been required or suggested in that manual can be applied only to the real time data:  
856 the application of the gap test needs the time stamp of each measurement, the application of the  
857 syntax test requires the full original data record, and the application of the neighbor test is possible  
858 only in the case when a nearby second sensor is installed on the device. Information needed for  
859 these tests is not kept in the WOD therefore these tests cannot be applied to “static” archive data.  
860 Five other tests outlined in B2015 are conceptually similar to the tests applied by our QC procedure:  
861 location test, gross range test, climatology test (all three required by B2015), spike test and flat line  
862 test (both recommended by B2015). In a deviation from our QC procedure, thresholds for test

863 variables according to B2015 should be chosen subjectively by operators in the data centers. We  
864 note that the metadata on decisions made operators are usually missing in the data archives.

865 The novelty of the proposed quality scheme is that the threshold choice is based on the  
866 respective statistics of test variables, and the Gaussian distribution is not assumed for the important  
867 local climatological range checks for oxygen and for oxygen vertical gradient. The QC procedure  
868 presented in this study was benchmarked against several hydrographic datasets known for their  
869 outstanding measurement quality, with WOCE experiment data collection being the largest and best  
870 documented. Analysis of the outliers and their distribution among distinct hydrographic sections  
871 and cruises suggests the ability of the procedure to flag outliers but retain the overwhelming  
872 majority of good data. The accompanying diagnostic tool provides the overview of outlier scores  
873 and permits tuning of thresholds when new benchmark quality-controlled datasets become  
874 available. Finally, we note that the transparent choice of test threshold values on the basis of the  
875 underlying statistics and the subsequent analysis of outliers for each quality check permits further  
876 tuning of the quality control procedure in order to increase the percentage of true outliers and to  
877 decrease the percentage of falsely identified outliers.

878 Further, we estimated possible residual oxygen biases in the delayed-mode adjusted Argo  
879 oxygen profiles. The bias estimates are based on the collocated Argo and discrete water sample  
880 ship-based profiles. The latter represents reference measurements as the bottle samples are analyzed  
881 by means of the Winkler chemical method. The size of the collocation bubble (e.g., the maximum  
882 distance between two profiles and the maximum time difference) was set at 100 km and 5 years,  
883 respectively, after several experiments with different bubble sizes. Residual biases relative to the  
884 Winkler reference data are represented by the difference at an isobaric level between the Argo  
885 sensor oxygen value and the Winkler oxygen, with the overall bias at each level being defined by  
886 the average of individual differences. To reduce the impact of time- and spatial variability, the final  
887 bias assessment is done for the layer 1000-1900m, which is typically located below the main  
888 thermocline.

889 Using all available Argo profiles which have collocations with reference Winkler data, we  
890 calculated overall oxygen offsets for six models of oxygen sensors implemented on Argo BGC  
891 floats and for six Argo DACs. Our results suggest that derived biases are both sensor- and DAC-  
892 specific, with the electrochemical SBI-series sensors exhibiting a positive bias in the range from 0.5  
893 to 2.6  $\mu\text{mol}/\text{kg}$ . The optoid sensors typically are characterized by negative biases ranging between -  
894 0.7 and -6.2  $\mu\text{mol}/\text{kg}$  depending on sensor model and DAC. Only for  
895 AANDERAA\_OPTODE\_3830 small positive offsets were found for AOML and CSIRO, as well as  
896 positive offsets for SBE63\_OPTODE for Coriolis and CSIRO. This diagnosed biases are crucial to

897 accurately identify the deoxygenation trend, as current assessments suggest an upper 1000 m O<sub>2</sub>  
898 content decrease of 0.2–1.2  $\mu\text{mol kg}^{-1} \text{dec}^{-1}$  during 1970–2010 (Gulev et al. 2023). Our calculations  
899 suggest that at least 1000 collocation pairs are needed for the stable residual bias estimation. This  
900 number of collocations is available only for AOML, Coriolis, JMA, CSIRO, INCOIS, and MEDS  
901 datasets.

902 Diagnosed residual biases for the quality-controlled CTD oxygen sensor profiles revealed a  
903 good agreement between the CTD and Winkler reference data, with a small median bias of 0.25  
904  $\mu\text{mol kg}^{-1}$  within the layer below 1000 m. Because of a relatively small bias value, which is well  
905 within the uncertainty of the CTD sensors and due to a non-uniform spatial CTD bias pattern, the  
906 diagnosed overall bias is not considered to be a common and robust feature, and no adjustment of  
907 CTD data is performed in this study. Our preliminary investigation also indicates that the CTD  
908 offset varies cruise-by-cruise, probably associated with the differences in the calibration or re-  
909 calibration (or post-processing). Therefore, the follow-on work should include investigating the  
910 offsets on a cruise-by-cruise basis and providing an understanding of the causes of bias. Only after  
911 these examinations are done can the adjustment of CTD profiles be physically tenable.

912 This study also has some limitations and caveats: (1) Although systematic errors have been  
913 identified for Argo oxygen data, the cause of the biases is still poorly known and requires further  
914 work. The differences between the DAC centers are also mysterious, and we suspect that the non-  
915 standard adjustment procedure developed by different National Argo Data Centers and the  
916 difference in sensors on Argo floats used in different countries might be responsible for the  
917 differences in diagnosed biases, which needs further confirmation. (2) Because the sources of biases  
918 are poorly known, the correction proposed in our study is largely empirical and only applies to the  
919 Argo data used in this study. If the Global Argo Data Center updates quality control and adjustment  
920 procedures, our bias corrections also require an update. (3) The QC procedure is designed to detect  
921 and flag the outliers. However, there are also risks of removing the “real extremes” in the ocean,  
922 especially under rapid climate change, as ocean extreme events are expected to become more  
923 frequent. One possible way to partly resolve this problem is imposing a trend in the local  
924 climatological range, accounting for the time-variation of the local oxygen distributions due to  
925 climate change, which would help to reduce the false rejection of the real extreme data. This  
926 requires further work when the local oxygen trends become clearer. (4) The Winkler data are used in  
927 this study as a reference. However, it is likely that the Winkler data are not always taken to the same  
928 standard, thus posing inconsistency within the Winkler dataset, especially for the data taken by  
929 different countries and in different time periods. Investigating offsets on a cruise-by-cruise basis is  
930 also recommended in the future, as for CTD data.

931 In summary, this study proposed a new quality control approach and bias assessment for the  
932 CTD, bottle, and Argo oxygen data and investigated the consistency between these three primary  
933 instrumentation types. Our investigations ensured the consistency between the three datatypes and  
934 provided a solid basis for merging them into a single, integrated, and homogeneous oxygen  
935 database. Therefore, the database obtained in this study supports the next-step assessment and  
936 understanding of the change in ocean oxygen levels.  
937

## 938 **9 Data availability**

939 The quality control procedure described above was applied to the OSD and CTD oxygen profiles  
940 between 1920 and 2023 from the World Ocean Database ([https://www.ncei.noaa.gov/access/world-](https://www.ncei.noaa.gov/access/world-ocean-database-select/dbsearch.html)  
941 [ocean-database-select/dbsearch.html](https://www.ncei.noaa.gov/access/world-ocean-database-select/dbsearch.html)) and to the oxygen profiles from the BGC Argo floats  
942 (<https://www.seanoe.org/data/00311/42182/>). The resulting dataset comprises observed level data  
943 with quality flags, and data interpolated on 10-meter levels. The data are in NetCDF format and  
944 include metadata information. The complete dataset (Gouretski et al., 2023) can be found at  
945 <http://dx.doi.org/10.12157/IOCAS.20231208.001> and  
946 [http://www.ocean.iap.ac.cn/ftp/cheng/IAP\\_oxygen\\_profile\\_dataset](http://www.ocean.iap.ac.cn/ftp/cheng/IAP_oxygen_profile_dataset)  
947

## 948 **10 Code availability**

949 The code of the QC system developed in this paper is available at  
950 [http://www.ocean.iap.ac.cn/ftp/cheng/IAP\\_oxygen\\_profile\\_dataset/QC\\_Code\\_SAMPLE.zip](http://www.ocean.iap.ac.cn/ftp/cheng/IAP_oxygen_profile_dataset/QC_Code_SAMPLE.zip).  
951

## 952 **Author contributions.**

953 LC and VG – conceptualization, supervision, methodology; VG – software, formal analysis, data  
954 validation, visualization, and writing (original draft preparation, final version, and editing); JD, XX,  
955 FC – methodology, data curation; LC – writing, analysis, methodology, funding acquisition; ZT –  
956 preparing data, formatting.  
957

958 **Competing interests.** The contact author has declared that none of the authors has any competing  
959 interests.  
960

961 **Acknowledgements.** We are thankful to the colleagues from the National Centers for  
962 Environmental Information (NCEI) and the Argo Global Assembly Center (GDAC) for providing  
963 access to the data used in this study (specific Argo DACs are noted in the text). We also thank two  
964 anonymous reviewers for their detailed and constructive comments. The Argo data were collected  
965 and made freely available by the International Argo Program and the national programs that  
966 contribute to it (ARGO, 2000). The Argo Program is part of the Global Ocean Observing System.

967

968 **Financial support.** This study was supported by the Strategic Priority Research Program of the  
969 Chinese Academy of Sciences [grant number XDB42040402], the National Natural Science  
970 Foundation of China [grant numbers 42122046 and 42076202], and the Youth Innovation  
971 Promotion Association, CAS [grant number 2020-077]. The author also acknowledges the support  
972 from the new Cornerstone Science Foundation through the XPLOER PRIZE, Youth Innovation  
973 Promotion Association, Chinese Academy of Sciences.

974

## 975 **References**

- 976 Adil, I. H. and Irshad, A. R.: A modified approach for detection of outliers, *Pak. J. Stat. Oper. Res.*,  
977 XI, 1, 91-102, 2015.
- 978 Argo (2024). Argo float data and metadata from Global Data Assembly Centre (Argo GDAC).  
979 SEANOE. <https://doi.org/10.17882/42182>.
- 980 Bittig, H. C., Maurer, T.L., Plant, J. N., Schmechtig, C., Wong, A. P. S., Claustre, H., Trull, T. W.,  
981 Udaya Bhaskar, T. V., Boss, E., Dall’Olmo, G., Organelli, E., Poteau, A., Johnson, K. S.,  
982 Hanstein, Leymarie, C., E., Le Reste, S., Riser, S. C., Rupan, A., Taillandier, V., Thierry, V. and  
983 Xing, X. : A BGC-Argo Guide: Planning, Deployment, Data Handling and Usage, *Front. Mar.*  
984 *Sci.*, 6:502, doi: 10.3389/fmars.2019.00502, 2018.
- 985 Baranova, O. K., Seidov, D., and Reagan, J. R.: World Ocean Atlas 2018, Volume 3: Dissolved  
986 Oxygen, Apparent Oxygen Utilization, and Oxygen Saturation. A. Mishonov Technical Ed.;  
987 NOAA Atlas NESDIS 83, 38pp, 2018.
- 988 Breitburg, D. et al. Declining oxygen in the global ocean and coastal waters. *Science* 359,  
989 eaam7240 (2018).
- 990 Bittig, H. C., and Körtzinger, A. (2015). Tackling oxygen optode drift: Near-surface and in-air  
991 oxygen optode measurements on a float provide an accurate in situ reference. *J. Atmos. Ocean.*  
992 *Technol.* 32, 1536–1543. doi: 10.1175/JTECH-D-14-00162.1

993 Boyer, T. P., Baranova, O.K., Coleman, C., Garcia, H. E., Grodsky, A., Locarnini, R. A., Mishonov,  
994 A. V., Paver, C. R., Reagan, J. R. , Seidov, D., Smolyar, I. V., Weathers, K., Zweng, M.M.:  
995 World Ocean Database 2018, A. V. Mishonov, Technical Editor, NOAA Atlas NESDIS 87,  
996 2018.

997 Bushnell, M., R. Toll., and H. Worthington: Manual for real-time quality control of dissolved  
998 oxygen observations: a guide to quality control and quality assurance for dissolved oxygen  
999 observations in coastal oceans, Integrated Ocean Observing System (U.S.), DOI :  
1000 <http://doi.org/10.7289/V5ZW1J4J>, 2015.

1001 Carpenter, J. H.: The accuracy of the Winkler method for dissolved oxygen analysis, *Limnology and*  
1002 *Oceanography*, 10, 1, p. 135-140. <https://doi.org/10.3419/lo.1965.10.1.0135>, 1965.

1003 Cheng, L. J., Zhu, J., Cowley, R., Boyer, T. and Wijffels, S.: Time, probe type and temperature  
1004 variable bias corrections to historical expendable bathythermograph observations, *J. Atmos.*  
1005 *Ocean. Technol.*,31, 1793–1825, doi:10.1175/JTECH-D-13-00197.1, 2014.

1006 Cheng, L., et al. Improved estimates of ocean heat content from 1960-2015. *Sci. Adv.* **3**, 3,  
1007 e1601545, <https://doi.org/advances.sciencemag.org/content/3/3/e1601545>, 2017.

1008 Cheng, L., Trenberth, K. E., Gruber, N., Abraham, J. P., Fasullo, J. T., Li, G., Mann, M. E., Zhao,  
1009 X., and Zhu, J.: Improved Estimates of Changes in Upper Ocean Salinity and the Hydrological  
1010 Cycle. *J. Climate*, 33, 10357-10381, <https://doi.org/10.1175/JCLI-D-20-0366.1>, 2020.

1011 Clark, L. C.: Cellophane/Platinum electrode for blood PO<sub>2</sub>, *J. Appl. Physiology*, 6, 189, 1953.

1012 Claustre, H., Johnson, K. S., and Takeshita, Y.: Observing the global ocean with biogeochemical-  
1013 Argo, *Annual Review of Marine Science*, 12, 23–48, 2020.

1014 Coppola, L., Salvetat, F., Delauney, L., Machoczek, D., Larstensen, J., Sparnocchia, S.,Thierry, V.,  
1015 Hydes, D., Haller, M.,Nair, R., Lefevre, D.: White paper on dissolved oxygen measurements:  
1016 scientific needs and sensors accuracy, 22 pages, 2013.

1017 Cowley, R., Killick, R. E., Boyer, T., Gouretski, V., Reseghetti, F., Kizu, S., Palmer, M. D., Cheng,  
1018 L., Storto, A., Le Menn, M., Simoncelli, S., Macdonald, A. M., and Domingues, C. M.:  
1019 International Quality-Controlled Ocean Database (IQuOD) v0.1: The Temperature Uncertainty  
1020 Specification, *Front. Mar. Sci.* 8:689695. doi: 10.3389/fmars.2021.6896, 2021

1021 Craig, H.: The GEOSECS program: 1972-1973: *Earth Planetary Science Letters*, v 23, p 63–64.,  
1022 1974

1023 Falck, E. and Olsen, A.: Nordic Seas dissolved oxygen data in CARINA, *Earth Syst. Sci. Data*, 2,  
1024 123–131, <https://doi.org/10.5194/essd-2-123-2010>, 2010.



1025 Baranova, O. K., Seidov, D., and Reagan, J. R.: World Ocean Atlas 2018, Volume 3: Dissolved  
1026 Oxygen, Apparent Oxygen Utilization, and Oxygen Saturation. A. Mishonov Technical Ed.;  
1027 NOAA Atlas NESDIS 83, 38pp, 2018.

1028 Deutsch, C., Brix, H., Ito, T., Frenzel, H. & Thomson, L. Climate-forced variability of ocean  
1029 hypoxia. *Science* **333**, 336–339, 2011.

1030 Golterman, H. L. The Winkler Determination. In: Gnaiger, E., Forstner, H. (eds) Polarographic  
1031 Oxygen sensors. Springer, Berlin, Heidelberg. [https://doi.org/10.1007/978-3-642-81863-9\\_31](https://doi.org/10.1007/978-3-642-81863-9_31),  
1032 pp.346-351, 1983.

1033 Garcia H. E., Z. Wang, C. Bouchard, S. L. Cross, C.R. Paver, J. R. Reagan, T. P. Boyer, R. A.  
1034 Locarnini, A.V. Mishonov, O. K. Baranova, D. Seidov, and D. Dukhovskoy. World Ocean  
1035 Atlas 2023, Volume 3: Dissolved Oxygen, Apparent Oxygen Utilization, Dissolved Oxygen  
1036 Saturation, and 30-year Climate Normal. A. Mishonov Technical Editor. *NOAA Atlas NESDIS*  
1037 *91*, 100 pp. <https://doi.org/10.25923/rb67-ns53> , 2024

1038 Good., S., Mills, B., Boyer T., Bringas, F., Castelão, G., Cowley, R., Goni, G., Gouretski, V. and  
1039 Domingues, C. M.: Benchmarking of automatic quality control checks for ocean temperature  
1040 profiles and recommendations for optimal sets, *Front. Mar. Sci.*, DOI  
1041 10.3389/fmars.2022.1075510, 2022.

1042 Gulev, S. et al. Changing state of the climate system. In *climate change 2021: The physical science*  
1043 *basis. Contribution of working group I to the sixth assessment report of the intergovernmental*  
1044 *panel on climate change (eds Masson-Delmotte, V. et al.). (Cambridge Univ. Press, 2021).*

1045 Gruber, N., Doney, S. C., Emerson, S. R., Gilbert, D., Kobayashi, T., Körtzinger, A., et al.. “Adding  
1046 oxygen to argo: Developing a global in situ observatory for ocean deoxygenation and  
1047 biogeochemistry,” in *Proceedings of Ocean Obs ‘09: Sustained Ocean Observations and*  
1048 *Information for Society*, eds J. Hall, D. E. Harrison, and D. Stammer (New Zealand: ESA  
1049 Publication), 12. doi: 10.5270/OceanObs09.cwp.39, 2010.

1050 Garcia H. E., Z. Wang, C. Bouchard, S.L. Cross, C.R. Paver, J.R. Reagan, T.P. Boyer, R.A.  
1051 Locarnini, A.V. Mishonov, O.K. Baranova, D. Seidov, and D. Dukhovskoy. World Ocean  
1052 Atlas 2023, Volume 3: Dissolved Oxygen, Apparent Oxygen Utilization, Dissolved Oxygen  
1053 Saturation, and 30-year Climate Normal. A. Mishonov Technical Editor. *NOAA Atlas NESDIS*  
1054 *91*, 100 pp. <https://doi.org/10.25923/rb67-ns53>, 2024

1055 Gruber, N. Warming up, turning sour, losing breath: ocean biogeochemistry under global change.  
1056 *Phil. Trans. R. Soc. A* 369, 1980–1996, (2011).

1057 Gouretski, V., Cheng, L., Du, J., Xing, X., Chai, F.: A quality-controlled and bias-adjusted global  
1058 ocean oxygen profile dataset, Marine Science Data Center of the Chinese Academy of  
1059 Sciences, <http://dx.doi.org/10.12157/IOCAS.20231208.001>, 2024.

1060 Gouretski, V.: World Ocean Circulation Experiment – Argo Global Hydrographic Climatology,  
1061 Ocean Sci., 14, 1127-1146, <https://doi.org/10.5194/os-14-1127-2018>, 2018.

1062 Gouretski, V. and Reseghetti, F.: On depth and temperature biases in bathythermograph data:  
1063 development of a new correction scheme based on analysis of a global database, Deep-Sea  
1064 Res., I, 57, 812-833, 2010.

1065 Gouretski, V. V., and Jancke, K.: Systematic errors as the cause for an apparent deep water property  
1066 variability: global analysis of the WOCE and historical hydrographic data., Prog. Oceanogr.,  
1067 48, 4, 337-402, 2000.

1068 Gregoire, M. et al.: A Global Ocean Oxygen Database and Atlas for Assessing and Predicting  
1069 Deoxygenation and Ocean Health in the Open and Coastal Ocean, Front. Mar. Sci., 8, 1-29,  
1070 <https://doi.org/10.3389/fmars.2021.724913> , 2021.

1071 Helm, K. P., Bindoff, N. L. & Church, J. A. Observed decreases in oxygen content of the global  
1072 ocean. *Geophys. Res. Lett.* **38**, L23602, 2011.

1073 Hood, E.M., Sabine, C.L., and M. Sloyan, B.M., eds.:The GO-SHIP Repeat Hydrography Manual:  
1074 A Collection of Expert Reports and Guidelines, IPCC Report Number 14, ICPO Publication  
1075 Series Number 134, 2010.

1076 Hubert, M. and Vandervieren, E.: An Adjusted boxplot for skewed distributions, Comput. Stat.  
1077 Data Anal., 52, 5186–5201, 2008.

1078 Keeling, R.F., Koetzinger, A., and Gruber, N.: Ocean Deoxygenation in a Warming world, Annu.  
1079 Rev. Mar. Sci., 2, 199-229. doi:10.1146/annurev.marine.010908.163855, 2010.

1080 Koertzinger, A., Schimanski, J., and Send, U.: High quality oxygen measurements from profiling  
1081 floats: A promising new technique, J. Atmos. Ocean. Technol., 22, 302-308, 2005.

1082 Ito, T., Minobe, A., Long, M. C. & Deutsch, C. Upper ocean O<sub>2</sub> trends: 1958–2015. *Geophys. Res.*  
1083 *Lett.* **44**, 4214–4223, 2017.

1084 Langdon, C.: Determination of Dissolved Oxygen in Seawater By Winkler Titration using  
1085 Amperometric Technique, The GO-SHIP Repeat Hydrography Manual: A Collection of Expert  
1086 Reports and Guidelines, Version 1, (eds Hood, E.M., C.L. Sabine, and B.M. Sloyan), 18pp..  
1087 (IOCCP Report Number 14; ICPO Publication Series Number 134), DOI:  
1088 <https://doi.org/10.25607/OBP-1350>, 2010.

1089 Larqué, L., Maamaatuaiahutapu, K., Garçon, V.: On the intermediate and deep water flows in the  
1090 South Atlantic Ocean. *Journal of Geophysical Research*, 102,C6,  
1091 <https://doi.org/10.1029/97JC00629>, 1997.

1092 Long, M. C., Deutsch, C. & Ito, T. Finding forced trends in oceanic oxygen. *Global Biogeochem.*  
1093 *Cycles* **30**, 381–397, 2016.

1094 Levin, L. A. Manifestation, drivers, and emergence of open ocean deoxygenation. *Annu. Rev. Mar.*  
1095 *Sci* **10**, 229–260 ,2018.

1096 Johnson, K. S., Plant, J., Coletti, L., Jannasch, H., Sakamoto, C., Riser, S., et al.. Biogeochemical  
1097 sensor performance in the SOCCOM profiling float array. *J. Geophys. Res. Oceans* 122, 6416–  
1098 6436. doi: 10.1002/2017JC01283, 2017

1099 Marks, R.: Dissolved oxygen supersaturation and its impact on bubble formation in the southern  
1100 Baltic Sea, *Hydrol. Res.*, 39,3, 229-236, 2008.Monhor, D. and Takemoto, S.: Understanding  
1101 the concept of outlier and its relevance to the assessment of data quality: Probabilistic  
1102 background theory, *Earth Planets Space*, 57, 1009–1018, 2005.

1103 Oschlies, A. et al. Patterns of deoxygenation - sensitivity to natural and anthropogenic drivers. *Phil.*  
1104 *Trans. Roy. Soc. A* **375**, 20160325, 2017.

1105 Praetorius, S. K. et al. North Pacific deglacial hypoxic events linked to abrupt ocean  
1106 warming. *Nature* **527**, 362–366, 2015.

1107 Pitcher, G. C., Aguirre, A., Breitburg, D., Cardich, J., Carstensen, J., Conley, D. J., et al. System  
1108 controls of coastal and open ocean oxygen depletion. *Prog. Oceanogr.* 197:102613. doi:  
1109 10.1016/j.pocean.2021.102613, 2021.

1110 Roemmich, D., Alford, M. H., Claustre, H., Johnson, K., King, B., Moum, J., et al. On the future of  
1111 Argo: An enhanced global array of physical and biogeochemical sensing floats. *Front. Mar. Sci.*  
1112 6:439. . doi: 10.3389/fmars.2019. 00439, 2019.

1113 Saout, C., Ganachaud, A., Maes, C., Finot, L., Jamet, L., Baurand, F., and Grilet, J. Calibration of  
1114 CTD oxygen data collected in the Coral Sea during the 2012 Bifurcation cruise. *Mercator*  
1115 *Ocean-Coriolis Quarterly Nesletter – Special Issue, #52-May*, 34-38, 2015.

1116 Sarachik, E.S.: CLIVAR: A Study of Climate Variability and Predictability: Science Plan. World  
1117 Climate Research Programme Report 89, WMO Technical Document No 690. 157 pp, 1995.

1118 Stramma, L., Oeschlies, A., and Schmidtko, S.: Mismatch between observed and modeled trends in  
1119 dissolved upper-ocean oxygen over the last 50 yr, *Biogeosciences*, 9, 4045–4057,  
1120 <https://doi.org/10.5194/bg-9-4045-2012>, 2012.

1121 Schmidtko, S., Stramma, L. & Visbeck, M. Decline in global oceanic oxygen content during the  
1122 past five decades. *Nature* **542**, 335–339, 2017.

1123 Taillander, V., Wagener, T., D'Ortenzio, F., Mayot, N., Legoff, Ras, H. J., Coppola, L., De  
1124 Fommervault, O. P., Schmechtig, C., Diamond, E., Bittig, H., Lefevre, D., Leymarie, E.,  
1125 Poteau, A., and Prieur A.: Hydrography and biogeochemistry dedicated to the Mediterranean  
1126 BGC-Argo network during a cruise with RV Tethys 2 in May 2015, *Earth Syst. Sci. Data*,  
1127 10, 627-641, 2018, <https://doi.org/10.5194/essd-10-627-2018>, 2018.

1128 Takeshita, Y., Martz, O. P., Johnson, K. S., Plant, J. N., Gilbert, D., Riser, S. C., Neil, C., and  
1129 Tilbrook, B.: A climatology-based quality control procedure for plotting float oxygen data, *J.*  
1130 *Geoph. Res: Oceans*, 118, 1-11, doi:10.1002/jgr.20399, 2013.

1131 Tan, Z., Cheng, L., Gouretski, V., Zhang, B., Wang, Y., Li, F., Liu, Z., Zhu, J.: A new automatic  
1132 quality control system for ocean profile observations and impact on ocean warming estimate,  
1133 *Deep-Sea Res. Part I: Oceanographic Research Papers*, 194,  
1134 <https://doi.org/10.1016/j.dsr.2022.103961>, 2023.

1135 Tengberg, A., Hovdenes, J., Andersson, H. J., Brocandel, O., Diaz, R., Hebert, D., Arnerich, T.,  
1136 Huber, C., Körtzinger, A., Khripounoff, A., Rey, F., Rönning, C., Schimanski, J., Sommer, S.  
1137 and Stangelmayer, A. : (2006): Evaluation of a lifetime-based optode to measure oxygen in  
1138 aquatic systems. *Limnol. Oceanogr.: Methods*, 4, 7-17, 2006.

1139 Thierry, V., Bittig, H., and the Argo-BGC team: Argo quality control manual for dissolved oxygen  
1140 concentration, Version 2.1, Argo Data Management, doi: <https://dx.doi.org/10.13155/46542>,  
1141 2021.

1142 Tukey, J. W. *Exploratory Data Analysis*, ed. Pierson, ISBN-10: 0201076160, 503 pp., 1977.

1143 Uchida, H., Johnson, G. C., and McTaggart, K. E.: CTD Oxygen sensor calibration procedures. *The*  
1144 *Go-SHIP Hydrography Manual: A Collection of Expert Reports and Guidelines*. IOCCP Report  
1145 No. 14, ICPO Publication Series No. 134, Version 1, 17p., 2010.

1146 WHPO: WOCE Operations Manual, Section 3.1.3: WHP operations and methods, WOCE report no.  
1147 69/91, WHPO 91-1. 80 pp., 1991.

1148 Winkler, L.: Die Bestimmung des in Wasser gelosten Sauerstoffes. *Berichte der Deutschen*  
1149 *Chemischen Gesellschaft*. 21 (2): 2843–2855. doi:10.1002/cber.188802102122, 1888.

1150 Wunsch, C.: *Towards the World Ocean Circulation Experiment and a bit of aftermath*, Springer-  
1151 Verlag, Jochum, M., Murtugudde, R., *Phys. Oceanogr.*, 181-201, 2006.

1152 Yang, J., Rahardja, S., and Fränti, P.: Outlier Detection: How to Threshold Outlier Scores?,  
1153 AIIPCC '19: Proceedings of the International Conference on Artificial Intelligence, Information  
1154 Processing and Cloud Computing, December 2019. Article No.: 37, p. 1–6  
1155 <https://doi.org/10.1145/3371425.3371427>, 2019.